Volume 25
Number 7
July 2023
Pages 1135–1254

# Environmental Science
## Processes & Impacts

rsc.li/espi

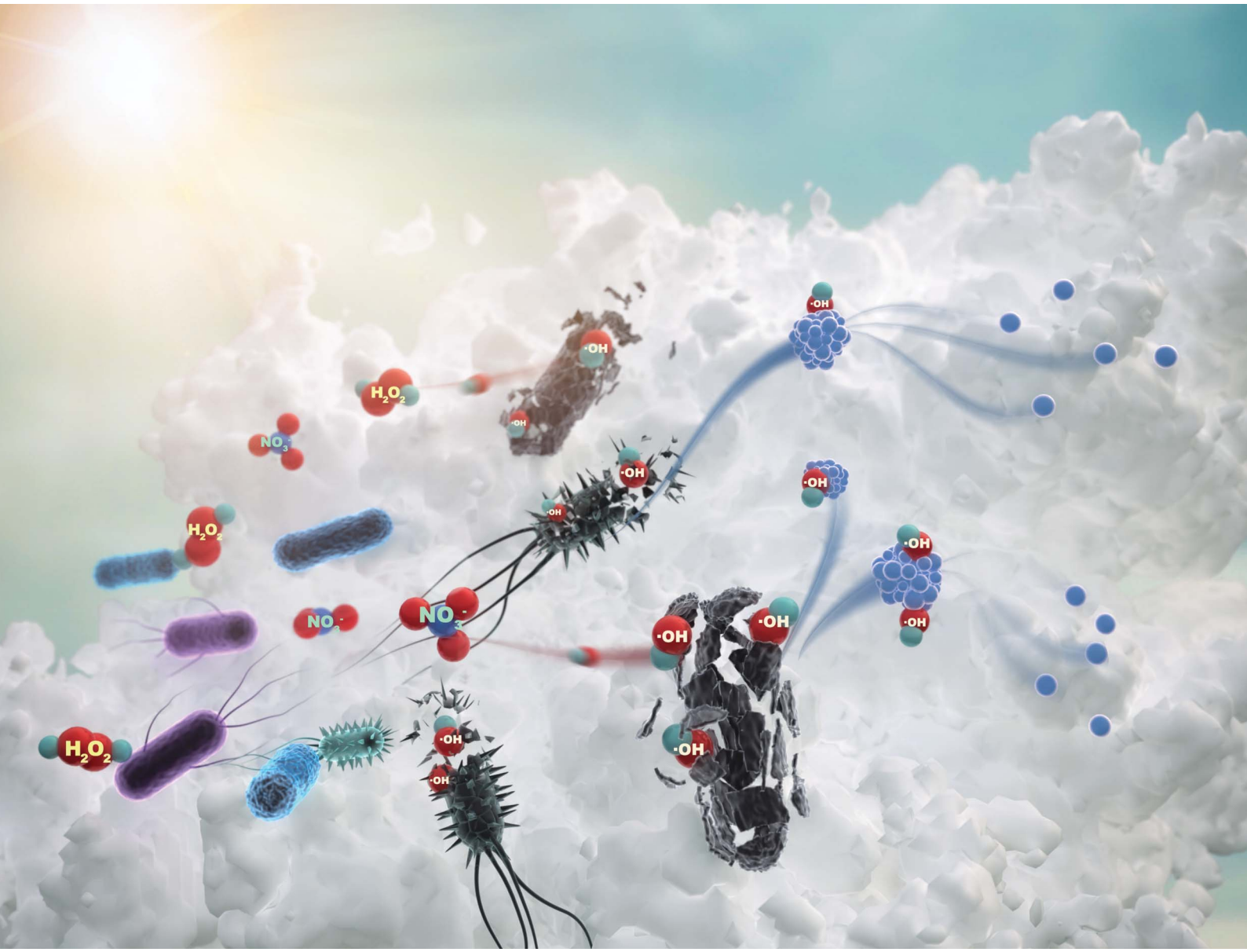


ISSN 2050-7887

**PAPER**
Theodora Nah *et al.*
Emerging investigator series: aqueous photooxidation of live bacteria with hydroxyl radicals under cloud-like conditions: insights into the production and transformation of biological and organic matter originating from bioaerosols

ROYAL SOCIETY OF CHEMISTRY

Environmental Science Processes & Impacts

PAPER

View Article Online
View Journal | View Issue

Check for updates

Cite this: *Environ. Sci.: Processes Impacts*, 2023, **25**, 1150

Open Access Article. Published on 08 June 2023. Downloaded on 5/21/2026 2:53:50 AM. This article is licensed under a Creative Commons Attribution 3.0 Unported Licence.

# Emerging investigator series: aqueous photooxidation of live bacteria with hydroxyl radicals under cloud-like conditions: insights into the production and transformation of biological and organic matter originating from bioaerosols†

Yushuo Liu,[ab] Patrick K. H. Lee[ac] and Theodora Nah *[abc]

Received 3rd March 2023
Accepted 7th June 2023

DOI: 10.1039/d3em00090g

rsc.li/espi

Live bacteria in clouds are exposed to free radicals such as the hydroxyl radical (•OH), which is the main driver of many photochemical processes. While the •OH photooxidation of organic matter in clouds has been widely studied, equivalent investigations on the •OH photooxidation of bioaerosols are limited. Little is known about the daytime encounters between •OH and live bacteria in clouds. Here we investigated the aqueous •OH photooxidation of four bacterial strains, *B. subtilis*, *P. putida*, *E. hormaechei* B0910, and *E. hormaechei* pf0910, in microcosms composed of artificial cloud water that mimicked the chemical composition of cloud water in Hong Kong. The survival rates for the four bacterial strains decreased to zero within 6 hours during exposure to $1 \times 10^{-16}$ M of •OH under artificial sunlight. Bacterial cell damage and lysis released biological and organic compounds, which were subsequently oxidized by •OH. The molecular weights of some of these biological and organic compounds were >50 kDa. The O/C, H/C, and N/C ratios increased at the initial onset of photooxidation. As the photooxidation progressed, there were few changes in the H/C and N/C, whereas the O/C continued to increase for hours after all the bacterial cells had died. The increase in the O/C was due to functionalization and fragmentation reactions, which increased the O content and decreased the C content, respectively. In particular, fragmentation reactions played key roles in transforming biological and organic compounds. Fragmentation reactions cleaved the C–C bonds of carbon backbones of higher molecular weight proteinaceous-like matter to form a variety of lower molecular weight compounds, including HULIS of molecular weight <3 kDa and highly oxygenated organic compounds of molecular weight <1.2 kDa. Overall, our results provided new insights at the process level into how daytime reactive interactions between live bacteria and •OH in clouds contribute to the formation and transformation of organic matter.

## Environmental significance

This work investigates the aqueous •OH photooxidation of four commonly found bacterial strains in microcosms composed of artificial cloud water that mimicked the chemical composition of atmospheric cloud water. The survival rates for the bacterial strains decreased to zero within 6 hours during exposure to •OH under artificial sunlight. Bacterial cell damage and lysis released biological and organic compounds, which were oxidized by •OH. Fragmentation reactions played a major role in driving the transformations of these compounds. The carbon backbones of higher molecular weight proteinaceous-like matter were cleaved to form a variety of lower molecular weight compounds, including HULIS and highly oxygenated organic compounds. These results provide new process-level and molecular-level insights into how daytime reactive interactions between live bacteria and •OH in clouds contribute to the formation and transformation of organic matter, which have important atmospheric and climate implications.

## 1 Introduction

Clouds serve as an important liquid reaction medium for aqueous-phase reactions of atmospheric organic and inorganic compounds.[1,2] Although the composition of inorganic compounds in clouds is currently pretty well-understood,[1] a large fraction of organic matter in clouds remains poorly

[a]*School of Energy and Environment, City University of Hong Kong, Hong Kong SAR, China. E-mail: theodora.nah@cityu.edu.hk; Tel: +852 3442 5578*

[b]*City University of Hong Kong Shenzhen Research Institute, Nanshan District, Shenzhen, China*

[c]*State Key Laboratory of Marine Pollution, City University of Hong Kong, Hong Kong SAR, China*

† Electronic supplementary information (ESI) available. See DOI: https://doi.org/10.1039/d3em00090g



This journal is © The Royal Society of Chemistry 2023

Open Access Article. Published on 08 June 2023. Downloaded on 5/21/2026 2:53:50 AM. This article is licensed under a Creative Commons Attribution 3.0 Unported Licence.

characterized. Chemical processes that contribute to the formation and transformation of organic matter in clouds remain an area of active research. Clouds also play important roles as a habitat for microorganisms to live in and as a medium for microbial processes.[3–7] Live microorganisms in the atmosphere originate primarily from natural sources.[8–10] Bacteria are one of the many types of live microorganisms that enter the atmosphere as primary biological aerosol particles ("bioaerosols"). Once they are aerosolized into the atmosphere, live bacteria can serve as cloud condensation nuclei and participate in cloud formation processes.[11–13] *Acinetobacter*, *Sphingomonas*, *Pseudomonas*, and *Bacillus* are some of the common cultivable live bacterial species that have been detected in clouds worldwide.[12,14–16]

After they have been incorporated into clouds, live bacteria are exposed to a range of atmospheric conditions that can have adverse effects on their survival and energetic states. Joly *et al.* (2015) previously examined how exposure to osmotic shocks, freeze–thaw cycles, and simulated sunlight individually impact the survival of different bacterial strains in microcosms simulating physicochemical cloud conditions at Puy de Dôme in France.[17] The authors reported that exposure to simulated sunlight had little effect on the survival rates of the bacterial strains, whereas exposure to osmotic shocks and freeze–thaw cycles negatively impacted the survival of the bacterial strains. Our recent study showed that the effect of sunlight exposure on the survival of bacteria will depend on the cloud water pH.[18] Using two *Enterobacter* strains in microcosms simulating cloud conditions at Tai Mo Shan in Hong Kong, we observed that exposure to simulated sunlight at pH 4 to 5 negatively impacted the energetic states and survival of the bacteria but the effects were minimal at pH > 5. Live bacteria are also exposed to oxidants in clouds. Previous studies have investigated how the survival and energetic states of bacteria are impacted by hydrogen peroxide,[6,17,19,20] which plays a central role in driving cloud chemistry since it is the main photochemical source of hydroxyl radicals (˙OH) in cloud water in most areas.[1] Exposure to hydrogen peroxide under dark conditions in microcosms mimicking cloud water at Puy de Dôme had little effect on the survival of *Pseudomonas graminis*, *Pseudomonas syringae*, and *Sphingomonas* sp. strains.[17] Changes in their energetic states indicated that the bacteria modulated some of their metabolic pathways as part of their response to the oxidative stress inflicted by hydrogen peroxide.[19,20]

There have been limited studies on the photooxidation of bioaerosols by ˙OH, which is the most important daytime oxidant free radical species in the troposphere.[21] ˙OH in cloud water can be due to mass transfer from the gas phase into the aqueous phase or *in situ* formation *via* dark Fenton processes and photochemical reactions of aqueous-phase photolabile inorganic and organic compounds (*e.g.*, hydrogen peroxide, nitrate, nitrite, and organic peroxides).[21–26] Even though the relative importance of these processes will impact the ˙OH concentration in cloud water, they are still not fully understood and remain an active area of research. Hydrogen peroxide and inorganic nitrate are the two main ˙OH photochemical sources in continental clouds.[1,26] The ˙OH photooxidation of atmospheric organic matter has been studied extensively. These ˙OH reactions proceed by either H atom abstraction or ˙OH addition to C=C bonds. Competition between reaction pathways that add oxygen-containing functional groups (functionalization) *vs.* cleave C–C bonds (fragmentation) during ˙OH photooxidation has a governing influence on the transformation of the composition of atmospheric organic matter. There have been some studies on the ˙OH photooxidation of biological molecules that serve as surrogates for bioaerosols. Bioaerosol surrogates usually used in these studies are known components of cells, and they include proteins, peptides, and lipids.[27–33] Past investigations on reactions of ˙OH with model protein systems found that the first step is typically H atom abstraction by ˙OH from C–H bonds located on amino acid side chains or the polypeptide backbone.[32,33] This leads to the functionalization of amino acid side chains, formation of protein–protein cross-linkages, and protein fragmentation. Past investigations on reactions of ˙OH with model polyunsaturated fatty acid systems showed that the first reaction step is primarily ˙OH addition to the C=C bonds to form hydroxyalkyl radicals.[28–30] These hydroxyalkyl radicals subsequently undergo intermolecular H atom abstraction reactions to form allylic alkyl radicals, which are key intermediates in functionalization reactions that form higher molecular weight compounds with carbonyl and hydroxyl functional groups on their carbon backbones. Despite these previous studies, our current understanding of the ˙OH photooxidation of bioaerosols remains lacking. This is because single-component model systems are typically used in these previous studies, whereas bacteria release a complex multi-component mixture of biological molecules.

At present, little is known about how daytime aqueous-phase encounters between ˙OH and live bacteria in clouds impact their survival rates and energetic states. Reactive encounters between ˙OH and the bacteria's cellular material may lead to cell damage, which can be lethal to the bacterial cells. These reactive encounters may also modify the bacteria's energetic states, cellular composition, and biological properties. These changes will affect the ability of the bacteria to biodegrade organic compounds, which in turn will impact the composition of organic matter and the organic carbon budget in clouds. In addition, our previous study showed that lipids, peptides, unsaturated hydrocarbons, nucleic acids, amino sugars, and carbohydrates can be released when bacteria are exposed to light under cloud-like conditions.[18] These released biological and organic molecules can subsequently react with ˙OH to form an array of higher and lower molecular weight organic compounds of different volatilities *via* functionalization and fragmentation reaction pathways. The lower volatility organic compounds will remain in cloud droplets while the more volatile organic compounds can partition between the gas phase and cloud droplets, which will impact the multiphasic organic carbon budget in clouds. Hence, understanding the daytime reactive encounters between ˙OH and live bacteria in clouds will help us better evaluate the impacts that live microorganisms have on organic matter production and transformation in

Open Access Article. Published on 08 June 2023. Downloaded on 5/21/2026 2:53:50 AM. This article is licensed under a Creative Commons Attribution 3.0 Unported Licence.

clouds, which have broad atmospheric and climate implications.

In this study, we investigate the aqueous ˙OH photooxidation of four bacterial strains under cloud-like conditions. The four bacterial strains belong to the *Bacillus*, *Pseudomonas*, and *Enterobacter* genera, which have been detected in atmospheric cloud water. *Bacillus* is a Gram-positive bacteria, whereas *Pseudomonas* and *Enterobacter* are Gram-negative bacteria. Laboratory experiments were conducted using microcosms that contained artificial cloud water that mimicked the chemical composition of cloud water at Tai Mo Shan in Hong Kong. Either hydrogen peroxide or inorganic nitrate was used as the aqueous ˙OH photochemical precursor. The main objectives of this study are to (1) investigate how daytime aqueous-phase interactions with ˙OH impact the survival and energetic states of live bacteria in clouds, (2) characterize the biological and organic compounds released from the bacteria during these interactions, and (3) investigate the competition between functionalization and fragmentation reactions in transforming the released biological and organic compounds as they undergo photooxidation.

## 2 Experimental methods

### 2.1. General approach

All the experiments were performed in microcosms mimicking the chemical composition of cloud water previously collected at the Tai Mo Shan station (TMS; 22°24′N, 114°16′E, 957 m a.s.l.), which is Hong Kong's highest point. This mountaintop site is influenced by both urban and regional continental pollution from the Pearl River Delta region and cleaner marine air masses from the western Pacific Ocean.[34] The chemicals used to prepare the artificial cloud water were acetic acid ($C_2H_4O_2$, Aldrich, ≥99.99%), formic acid ($CH_2O_2$, Fisher, ~98%), oxalic acid ($C_2H_2O_4$, Fluka, ≥99%), pyruvic acid ($C_3H_4O_3$, Merck, ≥99%), magnesium chloride ($MgCl_2 \cdot 6H_2O$, Merck, ≥99%), calcium chloride ($CaCl_2 \cdot 2H_2O$, Aldrich, 99%), potassium chloride (KCl, Merck, ≥99%), sodium chloride (NaCl, Merck, 99.5%), ammonium sulfate ($(NH_4)_2SO_4$, Merck, ≥99.5%), sodium hydroxide (NaOH, Merck, 99%) and hydrochloric acid (HCl, Acros Organics, ≥95%). The composition of inorganic and organic ions in the artificial cloud water medium and their mean concentrations measured at Tai Mo Shan are shown in Table S1.† The organic compounds (*i.e.*, formate, acetate, pyruvate, and oxalate) were selected for their abundance in cloud water at Tai Mo Shan.[34] The pH of the artificial cloud water was set to 5.2, which is reportedly the global mean pH of cloud water.[35]

Four bacterial strains were used in this study: *Bacillus subtilis* ATCC 6051-U, *Pseudomonas putida* ATCC 23467, *Enterobacter hormaechei* B0910, and *Enterobacter hormaechei* pf0910. *Bacillus subtilis* ATCC 6051-U and *Pseudomonas putida* ATCC 23467 were purchased from the American Type Culture Collection. Both *B. subtilis* and *P. putida* bacteria are commonly found in outdoor and indoor environments.[36,37] *Enterobacter hormaechei* B0910 and *Enterobacter hormaechei* pf0910 were isolated from an ambient air sample collected in Hong Kong. Details of their genomes can be found in our previous study.[18] The four bacterial strains were grown in nutrient broth (NB) at 30 °C to the stationary phase. The culture was subsequently centrifuged at 6000 rpm for 10 min at 4 °C, and the cell pellets were rinsed with artificial cloud water three times. Since *B. subtilis* is a spore-forming bacteria, we performed some experiments to investigate the interactions between ˙OH and *B. subtilis* endospores. Section S1† describes how the *B. subtilis* ATCC 6051-U endospores were prepared for experiments. The bacterial cells/endospores were re-suspended in artificial cloud water to an initial concentration of either $\sim 10^5$ cells per mL or $\sim 10^7$ cells per mL for experiments. Calibration curves were used to convert optical density to the bacterial cell/endospore concentration.

All the experiments were performed in three custom-built quartz reactors that had lids with vents to allow air to enter/exit the reactors. The initial volume of the solution in each reactor was 300 mL. The solutions were mixed continuously during each 12 hour experiment using a magnetic stirrer. The solutions were irradiated through a quartz window in each reactor with simulated sunlight produced by a 300 W Xenon lamp (GZYY300W, Yuye Co.) equipped with a long-pass filter of 3.3 mm thickness and wavelength cut-off at 300 nm (ZJB300, Taizhu Co.). The photon flux inside the reactors is shown in Fig. S1.† The photon flux falls in the range of 300 to 700 nm, with a maximum at 545 nm. The temperatures of the solutions (25 °C) were regulated using a fan aimed at the reactors. The solutions were mixed with either hydrogen peroxide ($H_2O_2$, Fisher, 36.5%) or sodium nitrate ($NaNO_3$, Fisher, ≥99.5%), which served as the ˙OH photochemical precursor. The $NO_3^-$ ion concentration (200 μM) in the solutions falls within the range of the $NO_3^-$ concentrations previously measured in atmospheric cloud water at Tai Mo Shan.[34] The $H_2O_2$ concentrations in atmospheric cloud water at Tai Mo Shan are not known. However, the $H_2O_2$ concentration (10 μM) in the solutions falls within the range of $H_2O_2$ concentrations reported in atmospheric cloud water in other locations that, like Tai Mo Shan, are subjected to both continental pollution and clean marine air masses, such as the Puy de Dôme in France (0.1 to 57.7 M) and Mont Schmücke in Germany (0.4 to 17 M).[38–40]

To investigate the composition of molecular weight-fractionated compounds released by bacteria, one set of experiments was performed wherein ultrafiltration was first applied to the solution aliquots to obtain molecular weight-fractionated filtrates, which were then subjected to total organic carbon, total nitrogen, and excitation–emission matrix fluorescence analyses (Section 3.3). In this set of experiments, the bacterial cells were re-suspended in artificial cloud water to an initial concentration of $\sim 10^7$ cells per mL to ensure that there was sufficient material in the molecular weight-fractionated filtrates for chemical analysis. In the second set of experiments wherein ultrafiltration was not performed prior to bulk compositional chemical analyses using ultra-performance liquid chromatography-mass spectrometry, size exclusion chromatography, and excitation–emission matrix fluorescence measurements (Section 3.2), the bacterial cells were re-suspended in artificial cloud water to an initial concentration of $\sim 10^5$ cells per mL. The same composition of the artificial cloud water medium (Table S1†) was used in these experiments

 This journal is © The Royal Society of Chemistry 2023

Open Access Article. Published on 08 June 2023. Downloaded on 5/21/2026 2:53:50 AM.
This article is licensed under a Creative Commons Attribution 3.0 Unported Licence.

regardless of the initial bacterial concentration used. The inorganic and organic ion concentrations in the artificial cloud water medium were not increased by 100 times in the experiments that used an initial bacterial concentration of $\sim 10^7$ cells per mL. This is because doing so resulted in high organic carbon and total nitrogen backgrounds, which interfered with the measurements of the total organic carbon and total nitrogen in the molecular weight-fractionated filtrates. Nevertheless, the bacterial survival rates measured in experiments using $\sim 10^7$ cells per mL initial cell concentrations were similar to those measured in experiments using $\sim 10^5$ cells per mL initial cell concentrations. This indicated that using a different initial concentration ratio of the chemical compounds in the artificial cloud water to bacterial cells did not affect the bacterial survival rates under our experimental conditions. This in turn suggested that the observed trends in the chemical compositional changes for the molecular weight-fractionated filtrates in experiments using $\sim 10^7$ cells per mL initial cell concentrations could be extrapolated to experiments using $\sim 10^5$ cells per mL initial cell concentrations. Control experiments were also performed using solutions that did not contain $H_2O_2$/$NaNO_3$. In dark control experiments, the reactors were covered completely with aluminum foil. All the experiments and measurements were performed in triplicate.

During each experiment, aliquots of the solution were removed from the reactors at different time points for offline analysis. At each time point, 100 μL of the solution was used for colony forming unit (CFU) counts on NB agar at 30 °C for 16 hours to determine the cell concentrations, which were used to calculate the bacterial survival rates. 20 μL of the solution was used for adenosine diphosphate/adenosine triphosphate (ADP/ATP) ratio measurements, which were used to monitor changes in the energetic states of bacteria. The ADP/ATP ratios were measured using an assay kit (EnzyLightTM, BioAssay Systems) and a bioluminometer (SpectraMax M2e, Molecular Devices) to monitor changes in the energetic states of bacteria. A constant ADP/ATP ratio can serve as an indication that the bacterial cells are growing since ADP (the degradation product of ATP) is constantly being converted to ATP to maintain ATP concentrations. In contrast, the ADP/ATP ratio will increase when the metabolism of ATP production is disrupted. This is because ADP cannot be converted to ATP even if ADP is still being formed from ATP. A live cell typically has an ADP/ATP ratio of around 0.25, while a dead cell has an ADP/ATP ratio of around 6.[41] Varying solution volumes were removed from the reactors for various chemical analyses as described in Section 2.2.

The biological analyses that were performed in this study, while essential for evaluating various aspects of microbial growth and activity, are not without limitations. For instance, the primary limitation of utilizing CFU counts on NB agar is its reliance on the ability of individual cells to form visible colonies on the agar surface. This method may not accurately reflect the total cell concentration as some viable cells may fail to form colonies due to factors such as cell aggregation, nutrient limitations, or the presence of viable but non-culturable (VBNC) cells. The assessment of cellular energetic states through the measurement of the ADP/ATP ratio also has drawbacks. This method assumes a direct relationship between the ADP/ATP ratio and the metabolic state of the cell, but this correlation may not always be consistent across different cell types or under varying growth conditions.

Separate experiments were performed using benzoic acid ($C_6H_5COOH$, J&K Scientific, 99.5%) as the $^{\bullet}OH$ probe compound to estimate the steady-state $^{\bullet}OH$ concentration ($[^{\bullet}OH]_{ss}$) in experiments initiated by the photolysis of 10 μM $H_2O_2$ or 200 μM $NO_3^-$. These experiments were performed using artificial cloud water solutions that did not contain bacterial cells. Details of the experimental methodology of these experiments can be found in our previous studies.[42–44] The estimated $[^{\bullet}OH]_{ss}$ values were found to be $0.99 \times 10^{-16}$ M and $0.95 \times 10^{-16}$ M for experiments initiated by 10 μM $H_2O_2$ photolysis and by 200 μM $NO_3^-$ photolysis, respectively. The estimated values are at the lower end of the range of $^{\bullet}OH$ concentrations previously estimated for atmospheric cloud water from measurements of bulk cloud water samples and multiphase chemistry cloud models ($10^{-16}$ to $10^{-12}$ M).[22,23,45,46] It should be noted that $^{\bullet}OH$ concentrations simulated by multiphase chemistry cloud models are typically higher than those obtained from measurements since the models tend to underestimate radical sinks and consider the mass transfer of $^{\bullet}OH$ from the gas phase to the aqueous phase as an additional source.[45]

Some of the chemical compounds in the artificial cloud water (Table S1†) can react with $^{\bullet}OH$ (*e.g.*, carboxylic acids). Thus, separate experiments were performed to determine if the chemical compounds in the artificial cloud water served as substantial $^{\bullet}OH$ sinks during the photooxidation experiments. These experiments were performed using solutions composed of benzoic acid ($^{\bullet}OH$ probe compound) and a $^{\bullet}OH$ photochemical precursor (*i.e.*, 10 μM $H_2O_2$ or 200 μM $NaNO_3$) mixed in ultra-pure water that did not contain any other chemical compounds and bacterial cells. The estimated $[^{\bullet}OH]_{ss}$ values were found to be $1.23 \times 10^{-16}$ M and $1.12 \times 10^{-16}$ M for these experiments initiated by 10 μM $H_2O_2$ photolysis and by 200 μM $NO_3^-$ photolysis, respectively. This indicated that the chemical compounds in the artificial cloud water only reduced the $[^{\bullet}OH]_{ss}$ by around 19% and 15% in experiments initiated by 10 μM $H_2O_2$ photolysis and by 200 μM $NO_3^-$ photolysis, respectively. This suggested that the chemical compounds in the artificial cloud water were not substantial $^{\bullet}OH$ sinks and likely would not reduce the effect of $^{\bullet}OH$ on the bacteria and the reactions of $^{\bullet}OH$ with biological and organic compounds released by the bacteria.

## 2.2. Chemical analysis

**2.2.1. Extraction of water-soluble and water-insoluble compounds.** Each aliquot of solution extracted for chemical analysis was first passed through a 0.22 μm pore size PTFE syringe filter (Tianjin Jinteng Experiment Equipment Co. Ltd, China) to remove intact bacterial cells. Water-soluble (WS) and water-insoluble (WIS) compounds were then extracted from these filtered solutions using the method described in Section S2.†

Open Access Article. Published on 08 June 2023. Downloaded on 5/21/2026 2:53:50 AM. This article is licensed under a Creative Commons Attribution 3.0 Unported Licence.

**2.2.2. Ultra-performance liquid chromatography-mass spectrometry analysis.** 200 μL of the extract was transferred into glass vial inserts for ultra-performance liquid chromatography-mass spectrometry (UPLC-MS) analysis. Non-targeted UPLC-MS analysis was performed using an ultrahigh performance liquid chromatography system (ExionLC AD system, Sciex, USA) coupled to a high-resolution quadrupole-time-of-flight mass spectrometer (TripleTOF 6600 system, Sciex, USA) equipped with electrospray ionization (ESI). Chromatographic separation was achieved using a Kinetex HILIC LC column (100 × 2.1 mm, 2.6 μm, 100 Å, Phenomenex, USA) and a gradient program. The information dependent analysis (IDA) acquisition was acquired with MS scan (100 to 1200 *m*/*z*) followed by MS/MS scan (50 to 1200 *m*/*z*) in positive and negative ion modes. The sample injection volume was 10 μL, and the flow rate was fixed at 0.3 mL $min^{-1}$ with ultra-pure water containing 5 mM ammonium acetate (Fisher, LC-MS grade) as mobile phase A and acetonitrile (Duskan, LC-MS grade) for mobile phase B. The raw MS data were processed for peak detection, retention time correction, alignment, and integration using the R package of PatRoon.[47] The O/C ratio, H/C ratio, N/C ratio, and double-bond-equivalent (DBE) values were calculated for each identified molecular formula. The UPLC-MS gradient program, operation parameters, data processing, and statistical analysis are described in Section S3.†

**2.2.3. Molecular weight-fractionated analysis by size exclusion chromatography.** 1 mL of the extract was used for molecular weight distribution analysis by size exclusion chromatography (SEC), which separates analyte molecules based on their molecular size. Separations were achieved using an SEC column (Polysep GFC P-3000, Phenomenex, USA) and a high-performance liquid chromatography system (Model 2695, Waters, USA) equipped with a photodiode array detector (Model 2998, Waters, USA). The chromatography system was operated in isocratic mode using a 90 : 10 v/v mixture of water and methanol (Duskan, HPLC grade) as the mobile phase, at a flow rate of 0.6 mL $min^{-1}$ and a sample injection volume of 20 μL. SEC separates analyte molecules based on their molecular size, with larger molecules eluting before smaller ones. The molecular weights of the analytes were empirically determined by comparing their elution volumes to those of sodium polystyrene sulfonate standards of known molecular weights from 1.6 to 68 kDa (Scientific Polymer Products Inc., USA). Molecular weight values derived from this calibration method are not definitive measurements, but rather estimations. This is because the calibration method relies on the assumption that the molecular densities of the calibration standard molecules are similar to those of the analyte molecules. However, the molecular densities of the standards may not be representative of those of analyte molecules, and interactions between the analyte molecules and the SEC column matrix may be different from those between the calibration standard molecules and the SEC column matrix.[48]

**2.2.4. Excitation–emission matrix fluorescence measurements.** 1 mL of the extract was used for light absorption measurements using a UV-visible absorption spectrophotometer (UV-33600, Shimadzu Corp., Japan). 1 mL of the extract was used for excitation–emission matrix (EEM) fluorescence spectroscopy measurements using a spectrofluorometer (FluoroMax-4, Horiba, Japan). Parallel factor analysis (PARAFAC) was performed on the EEM fluorescence spectra. Details of the EEM fluorescence measurements and PARAFAC analysis can be found in Section S4.†

**2.2.5. Ultrafiltration and characterization of molecular weight-fractionated water-soluble compounds.** To evaluate the composition of molecular weight-fractionated WS compounds released by the bacteria, 60 mL of the WS extract was filtered by ultrafiltration (Amicon® Ultra-15 centrifugal filter units, Merck Millipore Ltd, Ireland). Four centrifugal filter sizes were used: 3 kDa, 10 kDa, 30 kDa, and 50 kDa. Samples were separated within the 10 kDa, 30 kDa, and 50 kDa ultrafiltration units at 4000×*g* centrifugation for 10 min, while samples were separated within the 3 kDa unit at 4500×*g* centrifugation for 30 min. The filtrate from each filter size fraction was then used for EEM fluorescence (1 mL), total organic carbon (TOC) (9 mL), and total nitrogen (TN) (5 mL) measurements. A total carbon analyzer instrument (TOC-L CPH, Shimadzu, Japan) was used for TOC and TN measurements. The reported TOC and TN concentrations have been corrected for background TOC and TN from the artificial cloud water. Ultrafiltration could not be applied to WIS extracts.

# 3 Results and discussion

## 3.1. Impact of photooxidation on the survival and energetic states of bacteria

No significant changes in the survival rates and ADP/ATP ratios of *B. subtilis*, *P. putida*, *E. hormaechei* B0910, and *E. hormaechei* pf0910 were observed in the absence and presence of $H_2O_2$ or $NO_3^-$ under dark conditions (Fig. S2†). This indicated that exposure to $H_2O_2$ and $NO_3^-$ under dark conditions did not impact the survival and energetic states of the four bacterial strains under our experimental conditions. Similar to our findings that $H_2O_2$ exposure did not impact the survival rates of *B. subtilis*, *P. putida*, *E. hormaechei* B0910, and *E. hormaechei* pf0910, Wirgot *et al.* (2017, 2019) showed that $H_2O_2$ exposure under dark conditions in microcosms mimicking cloud water at Puy de Dôme did not impact the survival rates of *P. graminis*, *P. syringae*, and *Sphingomonas* sp. bacteria.[19,20] However, in contrast to our findings that $H_2O_2$ exposure did not impact the energetic states of *B. subtilis*, *P. putida*, *E. hormaechei* B0910, and *E. hormaechei* pf0910, Wirgot *et al.* (2017, 2019) reported that $H_2O_2$ exposure caused changes to the energetic states of *P. graminis*, *P. syringae*, and *Sphingomonas* sp. bacteria. It is unlikely that differences in the pH of the artificial cloud water used in our study (pH 5.2) and by Wirgot *et al.* (2017, 2019) (pH 6) contributed to the differences in our findings since these bacterial species are neutrophiles. Instead, the differences in our findings could partly be due to differences in the $H_2O_2$ concentrations used. 10 μM of $H_2O_2$ was used in this study, whereas Wirgot *et al.* (2017, 2019) used 20 μM and 200 μM $H_2O_2$ concentrations in their studies. The higher $H_2O_2$ concentrations used by Wirgot *et al.* (2017, 2019) may have elicited changes in the energetic states of their studied bacterial strains.

 This journal is © The Royal Society of Chemistry 2023

Open Access Article. Published on 08 June 2023. Downloaded on 5/21/2026 2:53:50 AM.
This article is licensed under a Creative Commons Attribution 3.0 Unported Licence.

It is also possible that the energetic states of different bacterial species (and strains) respond to $H_2O_2$ differently.

Fig. 1 shows the survival rates and ADP/ATP ratios of *B. subtilis*, *P. putida*, *E. hormaechei* B0910, and *E. hormaechei* pf0910 over time in the absence and presence of $H_2O_2$ or $NO_3^-$ under illumination conditions. In the absence of $H_2O_2$ and $NO_3^-$, there were no significant changes in the survival rates and ADP/ATP ratios of both *E. hormaechei* B0910 and *E. hormaechei* pf0910. This is consistent with results from our previous study where we showed that the survival rates and ADP/ATP ratios of *E. hormaechei* B0910 and *E. hormaechei* pf0910 will only change at pH < 5 under illumination

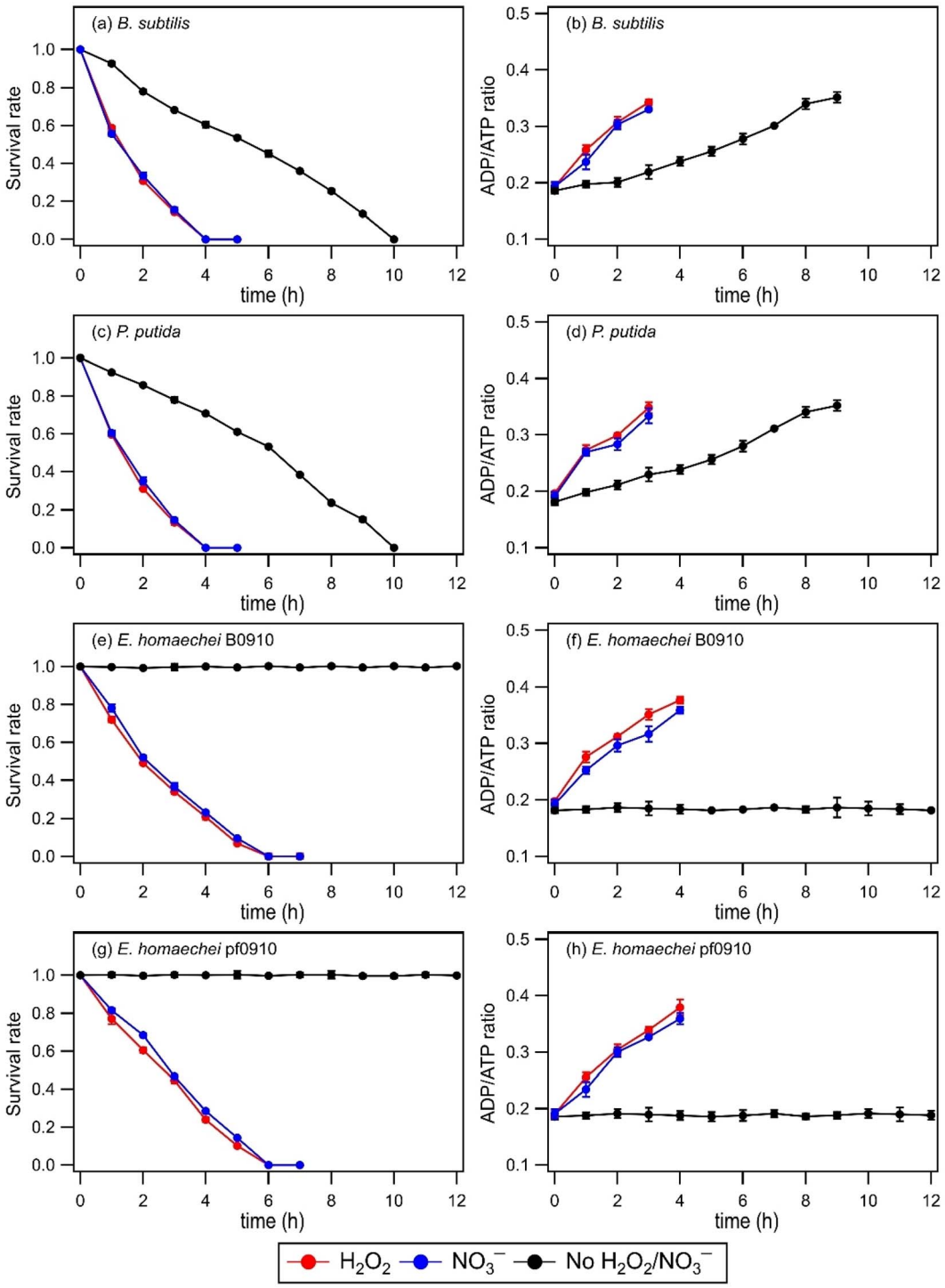


Fig. 1 (a, c, e, and g) Survival rates and (b, d, f, and h) ADP/ATP ratios of four bacterial strains in artificial cloud water in the absence and presence of $H_2O_2$ or $NO_3^-$ under illumination conditions over time. The survival rate is defined as the number concentration of culturable viable cells divided by the initial number concentration of culturable viable cells at time point 0 min. Error bars represent one standard deviation from the mean of biological triplicates.

Open Access Article. Published on 08 June 2023. Downloaded on 5/21/2026 2:53:50 AM. This article is licensed under a Creative Commons Attribution 3.0 Unported Licence.

conditions.[18] In contrast, exposure to light in the absence of $H_2O_2$ and $NO_3^-$ had a significant effect on the survival rates and ADP/ATP ratios of both *B. subtilis* and *P. putida*. The concentrations of their viable cells decreased to zero after 10 hours. Consistent with their decreasing survival rates, the ADP/ATP ratios of both *B. subtilis* and *P. putida* increased with time. This indicated that exposure to light caused cell damage and lysis in both *B. subtilis* and *P. putida*. Together, these results showed that exposure to light affected the four bacterial species differently at pH 5.2.

The presence of a $^{\bullet}OH$ photochemical precursor, $H_2O_2$ or $NO_3^-$, in the artificial cloud water medium had noticeable effects on the survival rates and ADP/ATP ratios of the four bacterial strains under illumination conditions. It took 4 hours for the concentrations of viable cells for both *B. subtilis* and *P. putida* to decrease to zero, as opposed to 10 hours when $H_2O_2$ or $NO_3^-$ was absent. The concentrations of viable cells for both *E. hormaechei* B0910 and *E. hormaechei* pf0910 also decreased to zero after 6 hours, as opposed to no significant changes in their survival rates when $H_2O_2$ or $NO_3^-$ was absent. Consistent with their decreasing survival rates, the ADP/ATP ratios for the four bacterial strains increased with time. The estimated $[^{\bullet}OH]_{ss}$ values were $0.99 \times 10^{-16}$ M and $0.95 \times 10^{-16}$ M in experiments that used $H_2O_2$ and $NO_3^-$ as $^{\bullet}OH$ photochemical precursors, respectively. Based on work by Lallement *et al.* (2018),[45] the bacterial cells are not expected to be a significant $^{\bullet}OH$ sink in our experiments due to the low initial bacterial cell concentrations used. Based on the decays in the survival rates of the four bacterial strains, the half-lives for *B. subtilis*, *P. putida*, *E. hormaechei* B0910, and *E. hormaechei* pf0910 were approximately 66 minutes, 64 minutes, 92 minutes, and 103 minutes, respectively. It should be noted that all the experiments were conducted at 25 °C, which is more representative of summer to early fall conditions in warmer regions such as Hong Kong.[34] Temperature is known to modulate microbial activity, including altering the rates at which the bacteria biodegrade organic compounds,[49] and the number of organic compounds biodegraded.[50] Thus, temperature will likely affect the survival rates and energetic states of the four bacterial strains as well.

Changes in the survival and energetic states of the four bacterial strains could be attributed to the presence of free radicals produced from the photolysis of $H_2O_2$ or $NO_3^-$. Aqueous-phase $H_2O_2$ photolysis only produces oxygen-containing free radicals $^{\bullet}OH$ and hydroperoxyl radicals ($HO_2^{\bullet}$), whereas aqueous-phase $NO_3^-$ photolysis produces nitrogen-containing free radicals nitrite ($NO_2^{\bullet}$) and nitroso ($^{\bullet}NO$) radicals in addition to $^{\bullet}OH$ and $HO_2^{\bullet}$.[21,26] Superoxide anion radicals ($O_2^{\bullet-}$) are also formed from the deprotonation of $HO_2^{\bullet}$ ($pK_a = 4.8$) under our experimental conditions.[21] These highly reactive free radicals can disintegrate the bacterial cell wall, inactivate the function of the bacterial cell membrane, and impair the functions of enzymes.[51] We expect $^{\bullet}OH$ to cause significant damage to most biological molecules due to its high reactivity. $HO_2^{\bullet}$ can also react with biological molecules, especially unsaturated lipids *via* peroxidation reactions.[52] $O_2^{\bullet-}$ are considered to be less reactive than $^{\bullet}OH$ but they can still cause cellular damage. More importantly, $O_2^{\bullet-}$ can react with other molecules to form more reactive species that can cause more substantial cellular damage.[53] Some of the free radicals (*e.g.*, $^{\bullet}NO_2$ and $^{\bullet}NO$) can also enter the cell membrane to react with functional biomolecules.[54] These processes likely contributed to the observed changes in the bacterial energetic states and cell death.

Experiments were also performed to investigate how exposure to $H_2O_2$ and $NO_3^-$ under dark and illumination conditions will affect the survival of *B. subtilis* endospores. No significant changes in the survival rates of *B. subtilis* endospores were observed (Fig. S3†). This could be attributed to the exterior structure of endospores, which allows them to tolerate stressors. The endospores likely resisted the free radicals because small, acid-soluble spore proteins bound to the DNA provided protection.[55] The low core water content in endospores may also have reduced the ability of stressors to generate intracellularly damaging free radicals.[55,56]

### 3.2. Chemical composition changes with photooxidation: bulk analysis

Fig. 1 clearly demonstrates that aqueous-phase $^{\bullet}OH$ and other reactive species produced from $H_2O_2$ or $NO_3^-$ photolysis significantly impact the survival and energetic states of bacteria. Since the abundance and chemical reactivity of $^{\bullet}OH$ are mostly higher than those of the other reactive species produced from the photolysis of $H_2O_2$ or $NO_3^-$, $^{\bullet}OH$ was likely the main reactive species that drove the observed changes in the bacterial survival and energetic states. The decreased survival rates are clear indications that cell damage and lysis occurred. Cell damage and lysis will lead to the release of biological and organic compounds, which can subsequently undergo photooxidation with $^{\bullet}OH$ and other reactive species (*e.g.*, $HO_2^{\bullet}$, $NO_2^{\bullet}$, $NO^{\bullet}$, $O_2^{\bullet-}$). EEM fluorescence spectroscopy and UPLC-MS were used to analyze the solution at different time points to investigate how these biological and organic compounds were transformed during photooxidation. No WS and WIS compounds were detected in $H_2O_2/NO_3^-$-containing solutions of the four bacterial strains under dark conditions, which is consistent with no significant changes in their survival rates under these conditions (Fig. S2†).

**3.2.1. EEM fluorescence measurements.** The EEM fluorescence measurements were used to provide insights into the evolution of the composition of fluorescent WS compounds released from the four bacterial strains during photooxidation. Four components were extracted from the EEM fluorescence spectra by PARAFAC analysis. They were identified based on comparisons of their PARAFAC-extracted EEM fluorescence spectra to those from previous bioaerosol studies (Table S2†). Components C1 and C2 were identified as proteinaceous-like matter, and they were assigned as tryptophan-like and tyrosine-like chromophores, respectively.[57,58] Tryptophan has a higher quantum yield than tyrosine,[58] so it is possible that tryptophan-like chromophores (component C1) have higher quantum yields than tyrosine-like chromophores (component C2). Components C3 and C4 were identified as humic-like substances (HULIS), and they were assigned as HULIS-1 and

 This journal is © The Royal Society of Chemistry 2023

Open Access Article. Published on 08 June 2023. Downloaded on 5/21/2026 2:53:50 AM. This article is licensed under a Creative Commons Attribution 3.0 Unported Licence.

HULIS-2 chromophores, respectively.[59,60] HULIS-2 chromophores (component C4) are less oxygenated than HULIS-1 chromophores (component C3).[60]

Fig. S4† shows the time evolution of the four components during photooxidation initiated by $H_2O_2$ and $NO_3^-$ photolysis. Components C1 and C2 increased at the initial onset of photooxidation (reaction time 0 to ~3 hour). Upon further photooxidation (reaction time beyond ~3 hour), components C1 and C2 decreased. The initial increase in components C1 and C2 could be attributed to the early stages of photooxidation being dominated by the release of proteinaceous-like matter from the bacteria as a result of cell damage and lysis. As the photooxidation progressed, reactions of the proteinaceous-like matter became increasingly important. The reactions of proteinaceous-like matter with free radicals may have occurred *via* H atom abstraction from C–H bonds located on amino acid side chains or the polypeptide backbone, which resulted in the functionalization of amino acid side chains, formation of protein–protein cross-linkages, and protein fragmentation.[32,33] These processes could have altered the abundance, composition, and fluorescent properties of the proteinaceous-like matter, which would explain the subsequent decreasing trends of components C1 and C2. By the time the concentrations of viable bacterial cells decreased to zero, reactions of the proteinaceous-like matter dominated. Components C3 and C4 increased continuously, albeit at slower rates during the later stages of photooxidation. The increase in components C3 and C4 could partly be attributed to the release of HULIS compounds from the bacteria as a result of cell damage and lysis. Part of the increase in components C3 and C4 could also be due to their formation from the photochemical reactions of proteinaceous-like matter such as tryptophan-like and tyrosine-like molecules.[61]

**3.2.2. UPLC-MS measurements.** The UPLC-MS measurements provided molecular-level information on the evolution of the composition of WS and WIS compounds released from the four bacterial strains during photooxidation. The peaks in the mass spectra generally fell in the $m/z$ range of 100 to 1200. The molecular formulae and signal intensities of the identified peaks (S/N $\geq$ 3) were used to calculate the intensity-weighted average values of the DBE and the X/C elemental ratios (X represents O, H, and N atoms) (Section S3†). Fig. 2 shows the time evolution of the intensity-weighted average DBE and X/C values during photooxidation initiated by $H_2O_2$ and $NO_3^-$ photolysis. The time evolution of the intensity-weighted average DBE and X/C values of the WS and WIS compounds released by the four bacterial strains showed similar trends. The DBE and X/C values increased at the initial onset of photooxidation (reaction time 0 to 1 hour). The increase in the DBE and X/C values coincided with the commencement of the decrease in the survival rates of the four bacterial strains (Fig. 1). The DBE, H/C, and N/C values were higher for the WIS compounds, whereas the O/C values were higher for the WS compounds. For example, in the case of *B. subtilis* with $H_2O_2$ as the $^{\bullet}OH$ photochemical precursor, the DBE, H/C, N/C, and O/C values for the WIS compounds were 4.43, 1.85, 0.21, and 0.30, respectively, at 4 h (time point at which the survival rate of *B. subtilis* first reaches zero), while the corresponding values for the WS compounds were 4.19, 1.71, 0.31, and 0.35, respectively. A plausible explanation for this observation is that the more oxygenated biological and organic compounds (*i.e.*, having higher O/C ratios) were more polar, which resulted in their higher water solubility.[62]

As the photooxidation progressed (reaction time beyond 1 hour), there were little changes in the H/C and N/C values. In contrast, the DBE and O/C values decreased and increased significantly, respectively. Changes in the DBE and O/C values continued for hours even after the concentrations of viable bacterial cells had decreased to zero. This is highlighted in Fig. S5 to S8,† which compare the intensity-weighted average DBE and X/C values for the four bacterial strains at two time points T1 and T2. T1 denotes the time point when the survival rate of the bacterial strain first reaches zero, while T2 denotes the time point that is 6 hours after T1. The differences in the H/C and N/C values at T1 *vs.* T2 were not statistically significant ($p > 0.05$, Student's $t$-test). In contrast, the increase in the O/C values from T1 to T2 was statistically significant ($p < 0.05$, Student's $t$-test). The O/C values for the four bacterial strains, on average, increased by 0.03 and 0.03 for the WIS compounds with $H_2O_2$ and $NO_3^-$ as the $^{\bullet}OH$ photochemical precursor, respectively. The O/C values for the four bacterial strains, on average, increased by 0.04 and 0.04 for the WS compounds with $H_2O_2$ and $NO_3^-$ as the $^{\bullet}OH$ photochemical precursor, respectively. The decrease in the DBE values from T1 to T2 was also statistically significant ($p < 0.05$, Student's $t$-test). The DBE values for the four bacterial strains, on average, decreased by 0.32 and 0.35 for the WIS compounds with $H_2O_2$ and $NO_3^-$ as the $^{\bullet}OH$ photochemical precursor, respectively. The DBE values for the four bacterial strains, on average, decreased by 0.34 and 0.37 for the WS compounds with $H_2O_2$ and $NO_3^-$ as the $^{\bullet}OH$ photochemical precursor, respectively.

The increase in the O/C with photooxidation could be attributed to functionalization reactions that added oxygen-containing functional groups to the biological and organic compounds released from the bacteria. The functionalization reactions would cause an increase in the abundance of O atoms. Fragmentation reactions could also have contributed to the increase in the O/C. Some of the fragmentation reactions could have fragmented the carbon backbone of biological and organic compounds *via* C–C bond cleavage to form small volatile molecules that escaped into the gas phase. This would result in a decrease in the abundance of C atoms, and thus an increase in the O/C. The decrease in the DBE with photooxidation indicated a decrease in the degree of unsaturation. This could be attributed to the preferential photooxidation of aromatic and unsaturated compounds *via* free radical addition to the C=C bonds and the preferential degradation of oligomeric compounds through photodissociation and reactions with free radicals.[63]

Differences in the intensity-weighted average DBE and X/C values for the WS and WIS compounds during photooxidation initiated by $H_2O_2$ photolysis *vs.* $NO_3^-$ photolysis were statistically insignificant ($p > 0.05$, Student's $t$-test) for all four bacterial strains. This implied that the $^{\bullet}OH$ photochemical precursor did not have a significant impact on how the composition of the

Open Access Article. Published on 08 June 2023. Downloaded on 5/21/2026 2:53:50 AM.
This article is licensed under a Creative Commons Attribution 3.0 Unported Licence.

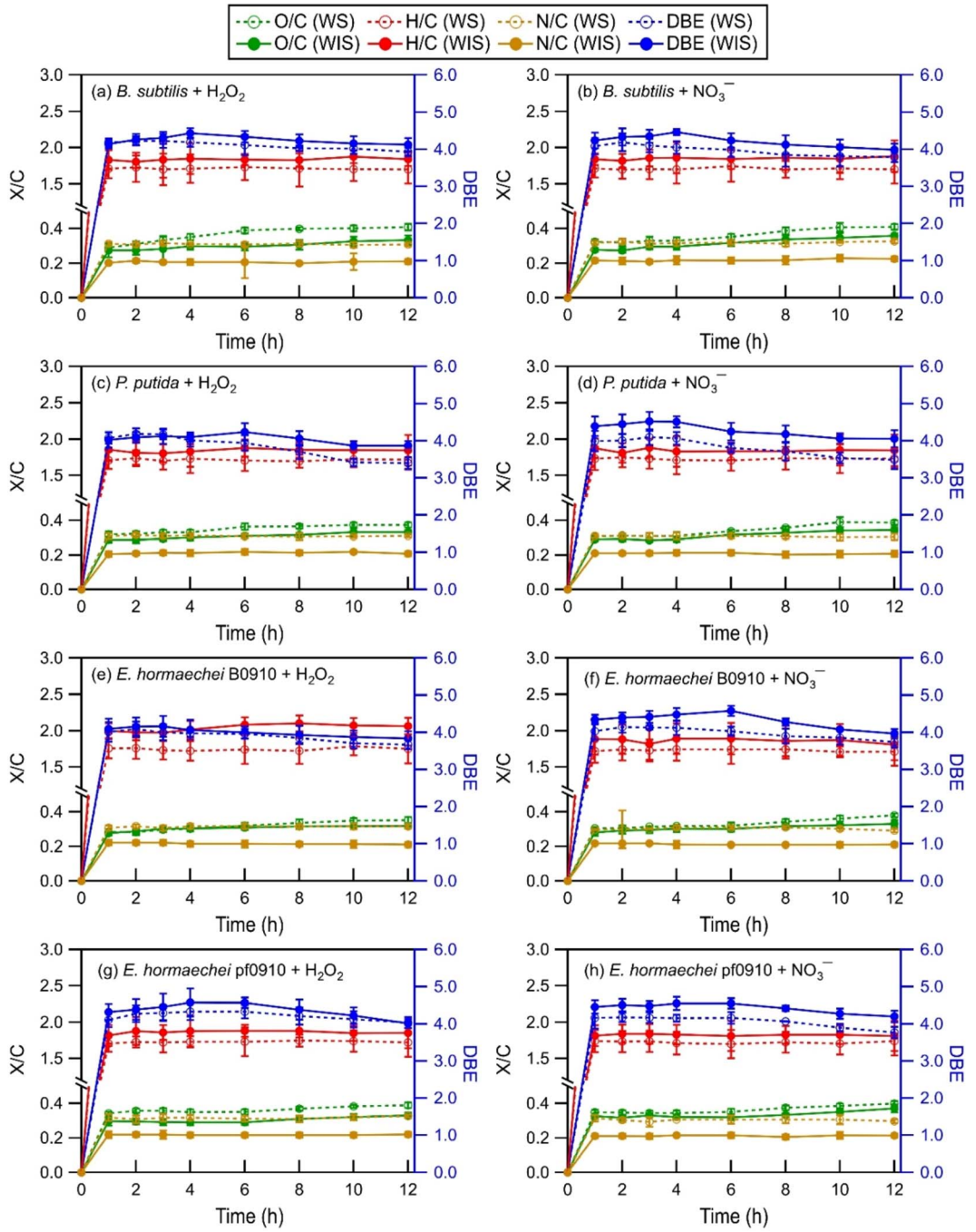


Fig. 2 Time evolution of the intensity-weighted average DBE, O/C, H/C, and N/C of WS and WIS compounds from the four bacterial strains during photooxidation initiated by the photolysis of (a, c, e, and g) $H_2O_2$ and (b, d, f, and h) $NO_3^-$. Error bars represent one standard deviation from the mean of triplicate measurements. Comparisons of the DBE, O/C, H/C, and N/C of WS and WIS compounds at time points T1 (*i.e.*, the time point when the survival rate of the bacterial strain first reaches zero) *vs.* T2 (*i.e.*, the time point that is 6 hours after T1) are shown in Fig. S5 to S8.†

released biological and organic compounds evolved as they underwent photooxidation under our experimental conditions. The statistically insignificant differences in the N/C ratios were somewhat surprising. This is because even though aqueous-phase $H_2O_2$ and $NO_3^-$ photolysis both produce $^{\bullet}OH$ and $HO_2^{\bullet}$, $NO_3^-$ photolysis also produces $NO_2^{\bullet}$ and $NO^{\bullet}$.[21,26] Roughly equal quantities of $NO_2^{\bullet}$ and $^{\bullet}OH$ are produced by $NO_3^-$ photolysis.[64,65] The statistically insignificant differences in the N/C ratios could be explained by $NO_2^{\bullet}$ and $NO^{\bullet}$ typically having lower chemical reactivities than $^{\bullet}OH$.[64–66] The reactions of $NO_2^{\bullet}$ and $NO^{\bullet}$ with biological and organic compounds are expected to proceed *via* similar mechanisms to the reactions of $^{\bullet}OH$ with biological and organic compounds. Analogous to the $^{\bullet}OH$ reactions, the reactions of $NO_2^{\bullet}$ and $NO^{\bullet}$ with saturated biological and organic compounds proceed *via* H atom abstraction, whereas the reactions of $NO_2^{\bullet}$ and $NO^{\bullet}$ with unsaturated

 This journal is © The Royal Society of Chemistry 2023

Open Access Article. Published on 08 June 2023. Downloaded on 5/21/2026 2:53:50 AM.
This article is licensed under a Creative Commons Attribution 3.0 Unported Licence.

biological and organic compounds proceed either by H atom abstraction or the addition of $NO_2^{\bullet}$ and $NO^{\bullet}$ to the C=C bond(s).[67,68] The addition of $NO_2^{\bullet}$ and $NO^{\bullet}$ to the C=C bond(s) of an unsaturated biological or organic compound could increase the number of N atoms in the compound. However, the statistically insignificant differences in the N/C ratios suggested that the reactions of unsaturated biological and organic compounds could have been dominated by $^{\bullet}OH$ due to its high reactivity.

Several methods have been used by the atmospheric community to graphically visualize and classify peaks in complex MS datasets based on the molecular formulae and elemental ratios of the peaks, including the Van Krevelen (VK) diagram (H/C *vs.* O/C),[69] carbon oxidation state *vs.* number of C atoms diagram,[70] and DBE *vs.* number of C atoms diagram.[71] To better understand how the composition of biological and organic compounds released from the four bacterial strains evolved during photooxidation, the O/C and H/C ratios of the

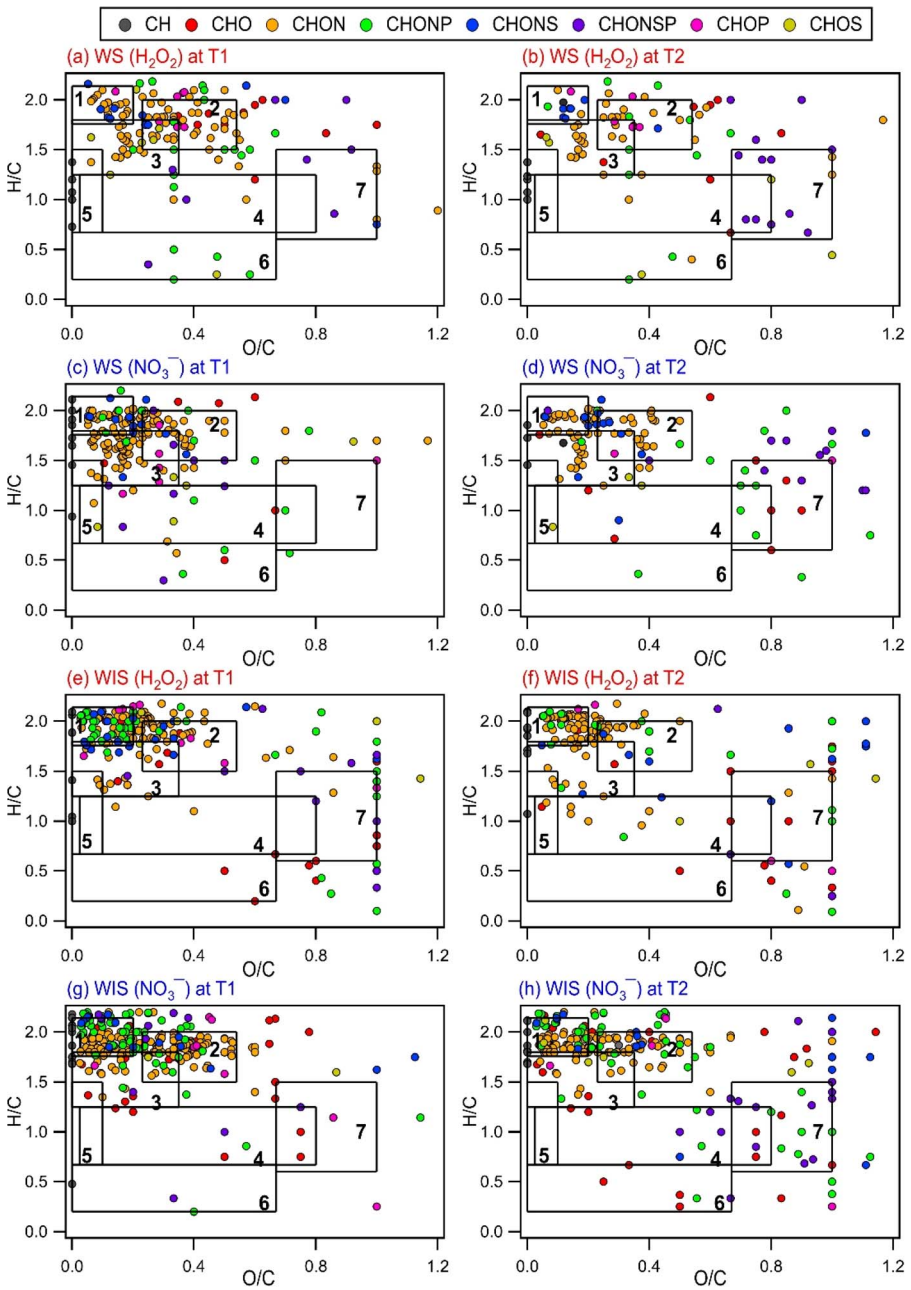


Fig. 3 VK diagrams of WS and WIS compounds from *B. subtilis* at time points T1 and T2 during photooxidation initiated by the photolysis of (a, b, e, and f) $H_2O_2$ and (c, d, g, and h) $NO_3^-$. Time point T1 is when the survival rate of the bacterial strain first reaches zero, and time point T2 is 6 hours after T1. The VK diagrams are divided into seven chemical classes based on their combined O/C and H/C ratios: (1) lipids, (2) peptides, (3) terpenoids, (4) polyketides, (5) unsaturated hydrocarbons, (6) aromatic structures, and (7) HOCs. The symbols are colored based on compositions (CH, CHO, CHON, CHONP, CHONS, CHONSP, CHOP, and CHOS).

Open Access Article. Published on 08 June 2023. Downloaded on 5/21/2026 2:53:50 AM. This article is licensed under a Creative Commons Attribution 3.0 Unported Licence.

identified WS and WIS compounds were visualized on VK diagrams, which is a commonly used tool to graphically visualize and classify compounds in cloud water.[50,72] The WS and WIS compounds were categorized into seven groups based on the region of the VK diagrams that they were in according to their combined O/C and H/C ratios. Using previously reported boundaries of regions in VK diagrams, we divided the VK diagrams into seven regions: lipids, peptides, terpenoids, polyketides, unsaturated hydrocarbons, aromatic structures, and highly oxygenated compounds (HOCs) (Table S2†). A weakness of our approach is the partial overlap of some of the categories (*e.g.*, peptides and terpenoids), which could lead to the incorrect classification of peaks that fall within these overlaps.[72]

Fig. 3 and S9 to S11† show the VK diagrams for the four bacterial strains at time points T1 and T2 during photooxidation initiated by $H_2O_2$ and $NO_3^-$ photolysis. The VK diagrams of the WS and WIS compounds show several similar characteristics. The majority of the detected WS and WIS compounds were categorized as peptides and lipids based on their placements in the VK diagrams. This was unsurprising since proteins, amino acids, and lipids are the main components of cell membranes. The identified compounds in the VK diagrams were also classified into eight major subcategories based on the elements in their molecular formulae: CH, CHO, CHON, CHONP, CHONS, CHONSP, CHOP, and CHOS. The majority of the compounds were categorized as CHON molecules (Fig. S12†), which was unsurprising since C, H, O, and N are the most abundant elements in living organisms.

Comparisons of the VK diagrams at time points T1 *vs.* T2 indicated that the number of compounds in the lipids, peptides, terpenoids, and unsaturated hydrocarbons categories decreased significantly during photooxidation from time points T1 to T2. For experiments where the photooxidation was initiated by $H_2O_2$ photolysis, the number of WS compounds in the lipids, peptides, terpenoids, and unsaturated hydrocarbons categories for the four bacterial strains decreased, on average, by 58%, 62%, 49%, and 26%, respectively. For experiments where the photooxidation was initiated by $NO_3^-$ photolysis, the number of WS compounds in the lipids, peptides, terpenoids, and unsaturated hydrocarbons categories for the four bacterial strains decreased, on average, by 62%, 60%, 52%, and 33%, respectively. The percentage decreases in the number of WIS compounds from T1 to T2 were mostly smaller compared to the corresponding percentage decreases in the number of WS compounds. For experiments where the photooxidation was initiated by $H_2O_2$ photolysis, the number of WIS compounds in the lipids, peptides, terpenoids, and unsaturated hydrocarbons categories for the four bacterial strains decreased, on average, by 32%, 28%, 31%, and 22%, respectively. For experiments where the photooxidation was initiated by $NO_3^-$ photolysis, the number of WIS compounds in the lipids, peptides, terpenoids, and unsaturated hydrocarbons categories for the four bacterial strains decreased, on average, by 36%, 26%, 32%, and 53%, respectively. The observed decreases suggested that compounds that were classified in these four categories were more susceptible to reactions.

Reactions of WS and WIS compounds during photooxidation are expected to be driven primarily by $^{\bullet}OH$ under our experimental conditions. Compounds with C=C bonds typically react quickly with $^{\bullet}OH$. Terpenoids and unsaturated hydrocarbons are classes of compounds with C=C bonds. Some peptides (*e.g.*, those with tryptophan and tyrosine residues) and lipids (*e.g.*, polyunsaturated fatty acids) also have C=C bonds. Thus, the presence of highly reactive compounds with C=C bonds in the lipids, peptides, terpenoids, and unsaturated hydrocarbons categories could explain why the number of WS and WIS compounds in these four categories decreased significantly during photooxidation from time points T1 to T2. It should be noted that this simple comparison method that we used to identify the compound categories that were more susceptible to reactions is not quantitative. This is because the peak intensities of many compounds in the mass spectra likely changed as a result of photooxidation but without the disappearance/formation of peaks.

Fig. 4 and S13† show the time evolution of the number of WS and WIS compounds detected during photooxidation initiated by $H_2O_2$ and $NO_3^-$ photolysis. The total number of WS and WIS compounds increased and then decreased with photooxidation. The time points when the number of WS and WIS compounds peaked were different. For *B. subtilis* and *P. putida*, the total number of WS and WIS compounds peaked at around the 4th hour of photooxidation, which coincided with the time point when their viable cell concentrations reached zero. For *E. hormaechei* B0910 and *E. hormaechei* pf0910, the total number of WS and WIS compounds peaked at around the 6th hour of photooxidation, which coincided with the time point when their viable cell concentrations reached zero. It is worth noting that for *B. subtilis* and *P. putida*, the total number of WS and WIS compounds increased almost continuously when $H_2O_2$ and $NO_3^-$ were not present in the illuminated solution (Fig. S14†). WS and WIS compounds were not detected for *E. hormaechei* B0910 and *E. hormaechei* pf0910 when $H_2O_2/NO_3^-$ was absent from the illuminated solution.

The initial increase in the total number of WS and WIS compounds during photooxidation initiated by $H_2O_2$ and $NO_3^-$ photolysis could be attributed to the early stages of photooxidation being dominated by the release of biological and organic compounds from the bacteria as a result of cell damage and lysis. Based on Fig. 4 and S13,† majority of the WS and WIS compounds released by the bacteria were categorized as lipids, peptides, and terpenoids according to their combined H/C and O/C ratios. As the photooxidation progressed, reactions of the released biological and organic compounds became increasingly important. By the time the concentrations of viable bacterial cells decreased to zero, reactions of the biological and organic compounds started to dominate. This could explain why the total number of WS and WIS compounds for the four bacterial strains peaked at time point T1, which is when their concentrations of viable cells first reached zero.

Depending on the molecular structure of the biological/organic compound, its reaction with $^{\bullet}OH$ will proceed either by H atom abstraction or by $^{\bullet}OH$ addition to C=C bonds. The reaction steps following the initial H atom abstraction or $^{\bullet}OH$

 This journal is © The Royal Society of Chemistry 2023

Open Access Article. Published on 08 June 2023. Downloaded on 5/21/2026 2:53:50 AM.
This article is licensed under a Creative Commons Attribution 3.0 Unported Licence.

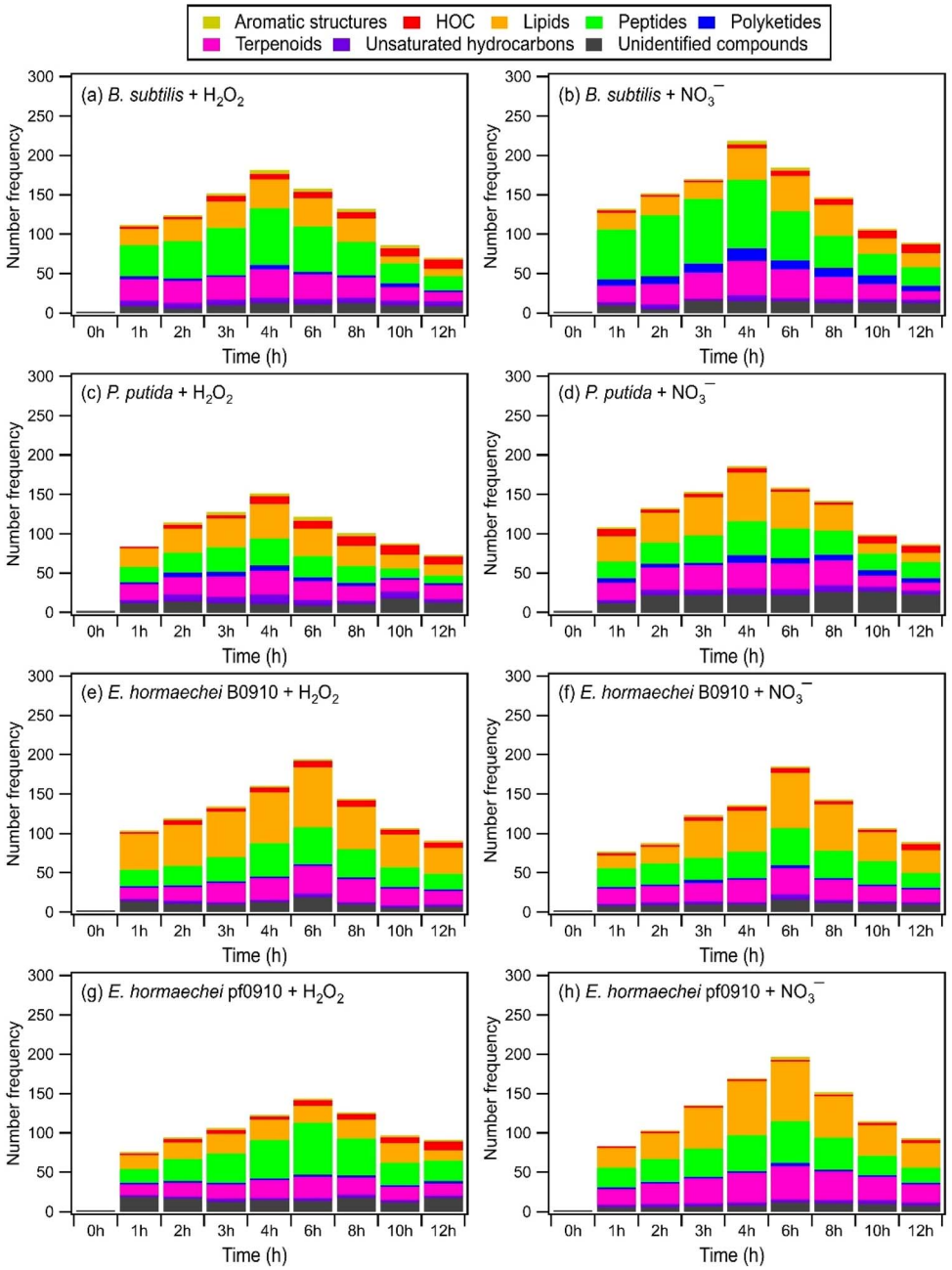


Fig. 4 Time evolution of the number of WS compounds from the four bacterial strains detected by UPLC-MS during photooxidation initiated by the photolysis of (a, c, e, and g) $H_2O_2$, and (b, d, f, and h) $NO_3^-$.

addition step will lead to the addition of polar, oxygen-containing functional groups (functionalization) and/or breaking of the carbon skeleton *via* C–C bond cleavage (fragmentation). UPLC-MS analysis was performed using a HILIC column, which is highly effective in separating polar compounds and is widely used in the proteomic and metabolomic fields to detect biomarkers, nucleosides, nucleotides, amino acids, peptides, and proteins.[73] Thus, our UPLC-MS methodology should allow us to detect compounds with added polar, oxygen-containing functional groups from both fragmentation and functionalization reactions. However, only compounds within the $m/z$ range of 100 to 1200 were detected. This indicated that compounds with molecular weights <100 Da formed from fragmentation reactions were not detected due to poor separation in UPLC and/or inefficient ionization by ESI. Fragmentation reactions could also have formed small volatile molecules that escaped into the gas phase and thus were not detected by UPLC-MS. Taken together, the decrease in the total number of WS and WIS compounds beyond time point T1 suggested that fragmentation reactions played a major role in the photooxidation.

Open Access Article. Published on 08 June 2023. Downloaded on 5/21/2026 2:53:50 AM.
This article is licensed under a Creative Commons Attribution 3.0 Unported Licence.

### 3.3. Chemical composition changes with photooxidation: molecular weight-fractionated analysis

Some biomolecules (*e.g.*, proteins) can have molecular weights >10 kDa. Since only compounds within the *m*/*z* range of 100 to 1200 were detected in UPLC-MS, this raised the question of whether UPLC-MS is an effective analytical method for detecting high molecular weight biological and organic compounds. To address this question, ultrafiltration was applied to the WS extracts to fractionate the compounds according to their molecular weights: <3 kDa, 3 to 10 kDa, 10 to 30 kDa, 30 to 50 kDa, and >50 kDa. Each filtrate was subsequently analyzed by UPLC-MS. For comparison purposes, we analyzed the molecular weight distributions of light-absorbing compounds in the WS extracts using SEC coupled to UV-visible absorption spectroscopy. While UPLC-MS detected biological and organic compounds in the <3 kDa filtrate, no compounds were detected in the 3 to 10 kDa, 10 to 30 kDa, 30 to 50 kDa, and >50 kDa filtrates. In contrast, the SEC/UV-visible absorption chromatograms showed that light-absorbing compounds as large as 68 kDa were released by the bacteria during photooxidation (Fig. S15†). The light absorbance intensities of higher molecular weight compounds typically peaked during the early stages of photooxidation, while the light absorbance intensities of lower molecular weight compounds peaked during the later stages of photooxidation. Overall, these results indicated that our UPLC-MS methodology could not detect high molecular weight biological and organic compounds effectively. This could be due to the low concentrations of individual high molecular weight biological and organic compounds (>3 kDa) produced during the photooxidation. The individual concentrations of these high molecular weight biological and organic compounds could be below the detection limit of the UPLC-MS instrument used in this study.

EEM fluorescence, TOC, and TN measurements were performed on the molecular weight-fractionated filtrates to provide insights into how the composition of molecular weight-fractionated compounds evolves during photooxidation. Fig. 5, S16 and S17† show the time evolution of the TOC and TN concentrations of molecular weight-fractionated filtrates of the four bacterial strains during photooxidation initiated by the photolysis of $H_2O_2$ and $NO_3^-$. The combined TOC and TN concentrations from the five molecular weight-fractionated filtrates increased before tapering off. The time points at which the combined TOC and TC concentrations started tapering off were associated with the bacterial survival rates. For *B. subtilis* and *P. putida*, the TOC and TN concentrations started to taper off at around the 4th hour of photooxidation, which coincided with when their survival rates reached zero. For *E. hormaechei* B0910 and *E. hormaechei* pf0910, the combined TOC and TN concentrations started to taper off at around the 6th hour of photooxidation, which coincided with when their survival rates reached zero.

Compounds with molecular weights >3 kDa were the main contributors to the combined TOC and TON concentrations in the 1st hour of photooxidation. However, the contributions of the five molecular weight-fractionated filtrates to the combined TOC and TON concentrations changed as the photooxidation progressed. The TOC and TON contributions of compounds in the 3 to 10 kDa, 10 to 30 kDa, and 30 to 50 kDa filtrates mostly increased and then decreased with photooxidation. Out of the three forementioned filtrates, the TOC and TON contributions of the 30 to 50 kDa filtrate peaked at the earliest reaction time, followed by the 10 to 30 kDa filtrate and then the 3 to 10 kDa filtrate. The TOC and TON contributions of the >50 kDa filtrate mostly decreased with photooxidation, whereas the TOC and TON contributions of the <3 kDa filtrate increased with photooxidation. The time evolution trends of the five molecular

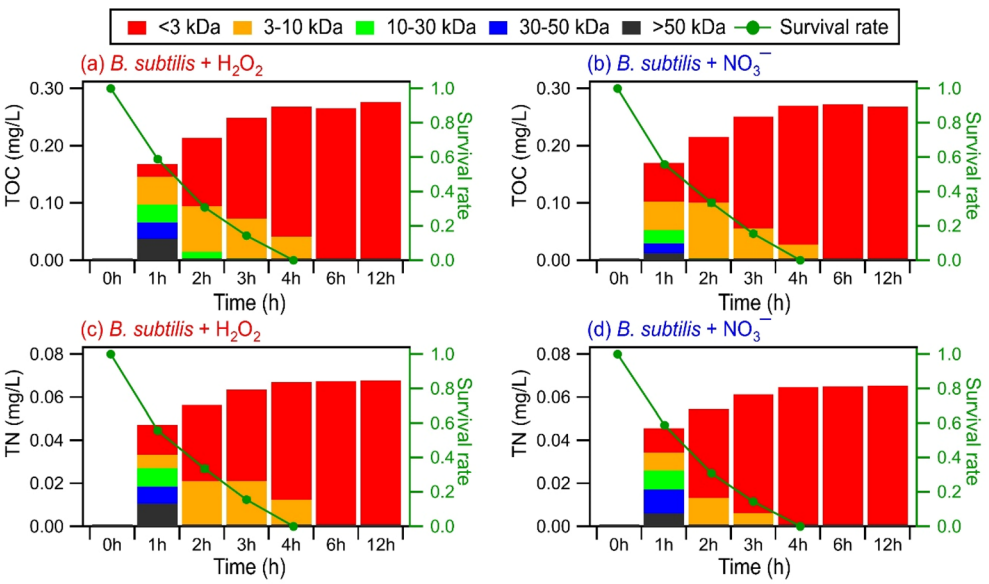


Fig. 5 TOC and TN concentrations of different molecular weight-fractionated (<3 kDa, 3 to 10 kDa, 10 to 30 kDa, 30 to 50 kDa, and >50 kDa) filtrates from *B. subtilis* during photooxidation initiated by (a and c) $H_2O_2$ and (b and d) $NO_3^-$ photolysis.

 This journal is © The Royal Society of Chemistry 2023

Open Access Article. Published on 08 June 2023. Downloaded on 5/21/2026 2:53:50 AM.
This article is licensed under a Creative Commons Attribution 3.0 Unported Licence.

weight-fractionated filtrates indicated that the lower molecular weight compounds mostly originated from fragmentation reactions of higher molecular weight compounds. There was little change in the TOC and TN concentrations of the <3 kDa filtrate from the 6th hour to the 12th hour of photooxidation. This was somewhat surprising since the total number of WS compounds detected by UPLC-MS decreased noticeably during the later stages of photooxidation (Fig. 4). This suggested that the decrease in the total number of WS compounds detected by UPLC-MS could be largely due to the fragmentation reactions forming small molecules that remained in the solution but were not detected by UPLC-MS due to poor separation in UPLC and/or inefficient ionization by ESI. However, we cannot discount the possibility that the instrument used for TOC and TN measurements was not sensitive enough to detect small decreases in the TOC and TN concentrations caused by the volatilization of small molecules formed from fragmentation reactions.

Fig. 6 and S18† show the time evolution of the four PARAFAC-extracted components in the five molecular weight-fractionated filtrates from the four bacterial strains during photooxidation initiated by the photolysis of $H_2O_2$ and $NO_3^-$. All the molecular weight-fractionated filtrates of the four bacterial strains contained the proteinaceous-like C1 and C2 components (tryptophan-like and tyrosine-like chromophores, respectively). In general, the C1 and C2 components in the five molecular weight-fractionated filtrates increased and then decreased with photooxidation. The time points at which the C1 and C2 components in the filtrates peaked were inversely correlated with the fractionated molecular weights. The >50 kDa filtrate peaked first, followed by the 30 to 50 kDa, 10 to 30 kDa, 3 to 10 kDa, and <3 kDa filtrates. This indicated that the lower molecular weight proteinaceous-like matter mostly originated from fragmentation reactions of higher molecular weight proteinaceous-like matter. These time evolution trends highlighted the important role that fragmentation reactions play in the photooxidation process.

Unlike the proteinaceous-like C1 and C2 components, the HULIS C3 and C4 components (HULIS-1 and HULIS-2 chromophores, respectively) were present mainly in the <3 kDa filtrate. This indicated that the HULIS components were present primarily as lower molecular weight compounds (<3 kDa). The C3 and C4 components in the <3 kDa filtrate increased before decreasing slightly at around the 8th hour of photooxidation. The increase in C3 and C4 components could be attributed in part to the release of HULIS compounds from the bacteria as a result of cell damage and lysis. Part of the increase in components C3 and C4 in the <3 kDa filtrate was also due to their formation from fragmentation reactions of higher molecular weight (>3 kDa) proteinaceous-like matter.[61] This would explain the small decrease in the C3 and C4 components during the later stages of the photooxidation since their formation from fragmentation reactions of higher molecular weight (>3 kDa) proteinaceous-like matter in the C1 and C2

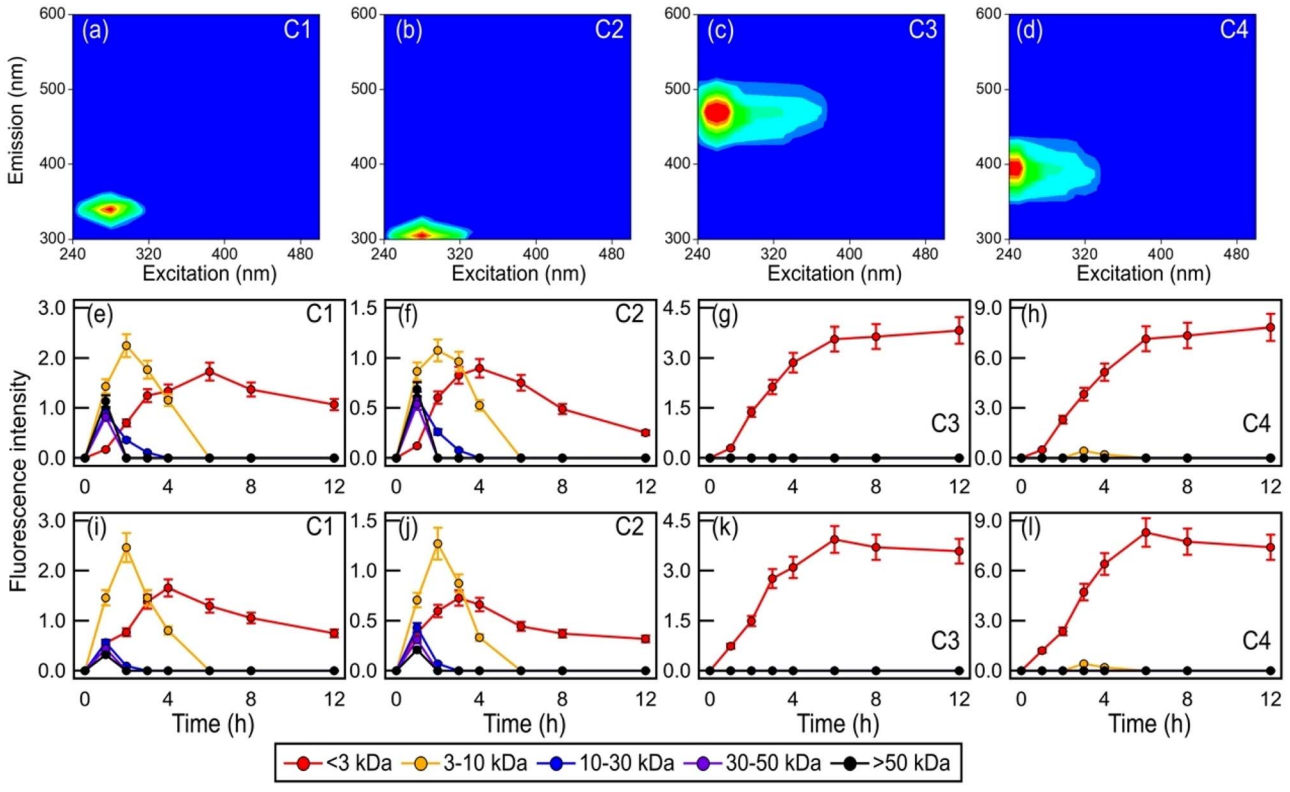


Fig. 6 (a to d) The PARAFAC-extracted EEM fluorescence spectra of components C1, C2, C3, and C4, which were assigned as tryptophan-like, tyrosine-like, HULIS-1, and HULIS-2 chromophores, respectively. Time evolution of the four PARAFAC-extracted components in the five molecular weight-fractionated filtrates from *B. subtilis* during photooxidation initiated by the photolysis of (e to h) $H_2O_2$ and (i to l) $NO_3^-$.

components mostly offset their decay caused by their reactions with ˙OH and other reactive species. The increase in the more oxygenated HULIS C3 component could also be partly due to its formation from functionalization reactions of the less oxygenated HULIS C4 component.[60]

# 4 Conclusions

In this study, we investigated the aqueous ˙OH photooxidation of four bacterial strains belonging to the *Bacillus*, *Pseudomonas*, and *Enterobacter* genera under cloud-like conditions at pH 5.2. Two of the four bacterial strains (*E. hormaechei* B0910 and *E. hormaechei* pf0910) were isolated from an ambient air sample collected in Hong Kong, while the other two bacterial strains (*B. subtilis* ATCC 6051-U and *P. putida* ATCC 23467) were from a culture collection. Even though the *B. subtilis* and *P. putida* strains used in this study were not isolated from atmospheric samples, our results are relevant to *B. subtilis* and *P. putida* strains found in atmospheric samples given the typically high similarities in genetic and physiological characteristics shared by the bacterial strains in the same genus. Our investigations showed that aqueous-phase interactions between ˙OH and live bacteria can have significant impacts on the bacterial survival and energetic states. Upon exposure to $1 \times 10^{-16}$ M ˙OH (and other reactive species) under artificial sunlight, the concentrations of viable cells for both *B. subtilis* and *P. putida* decreased to zero after 4 hours, while the concentrations of viable cells for both *E. hormaechei* B0910 and *E. hormaechei* pf0910 decreased to zero after 6 hours. This corresponded to half-lives of about 66 min, 64 min, 92 min, and 103 min for *B. subtilis*, *P. putida*, *E. hormaechei* B0910, and *E. hormaechei* pf0910, respectively. Our results imply that some bacterial species that are co-present with compounds that serve as ˙OH photochemical precursors in cloud droplets will not be able to survive for long periods of time during the day. The ˙OH concentrations in atmospheric cloud water typically range from $10^{-16}$ to $10^{-12}$ M.[46] Since the $[^{\cdot}OH]_{ss}$ in our experiments are on the lower end of the range of ˙OH concentrations in atmospheric cloud water, our experimentally-derived half-lives for *B. subtilis*, *P. putida*, *E. hormaechei* B0910, and *E. hormaechei* pf0910 against ˙OH represent an upper limit. It should be noted that the chemical composition (*e.g.*, ˙OH photochemical precursors), chemistry, and pH are not uniform across all cloud droplets;[74–76] thus the concentrations of ˙OH in different cloud droplets may span a wide range. For example, while ˙OH production from $H_2O_2$ photolysis does not depend significantly on the pH, the production of ˙OH and other free radicals from $NO_3^-$ photolysis depends strongly on the pH. Higher concentrations of ˙OH will be produced at lower pH during $NO_3^-$ photolysis as a result of higher ˙OH formation rates at lower pH.[42,77] In addition, all the experiments were conducted at 25 °C, which is more representative of summer to early fall conditions in warmer regions such as Hong Kong.[34] Since temperature can modulate microbial activity,[49,50] we expect temperature to also affect the half-lives of *B. subtilis*, *P. putida*, *E. hormaechei* B0910, and *E. hormaechei* pf0910 against ˙OH.

The damage and lysis of bacterial cells caused by the aqueous-phase interactions of live bacteria with ˙OH resulted in the release of a variety of biological and organic compounds, which underwent photooxidation with ˙OH (and other reactive species). Our chemical analysis revealed that the molecular weights of some of the released biological and organic compounds were >50 kDa. It should be noted that even though the duration of each experiment was set to 12 h to simulate a 12 h daytime period, the release and subsequent photooxidation of biological and organic compounds occurred at substantially shorter timescales. In all instances, biological and organic compounds were detected within the 1st hour of the experiment. This implied that the release of biological and organic compounds by live bacteria as a result of their aqueous-phase interactions with ˙OH would occur within the atmospheric lifetime of a cloud droplet. Furthermore, given that the $[^{\cdot}OH]_{ss}$ in our experiments are on the lower end of the range of ˙OH concentrations in atmospheric cloud water, the release and subsequent photooxidation of biological and organic compounds during aqueous-phase interactions between ˙OH and live bacteria in cloud droplets can potentially occur on timescales shorter than 1 h in the atmosphere.

UPLC-MS provided molecular-level insights into how biological and organic compounds with molecular weights <3 kDa were transformed during photooxidation. The O/C, H/C, and N/C ratios increased at the initial onset of photooxidation. As the photooxidation progressed, there were few changes in the H/C and N/C, whereas the O/C continued to increase for hours after all the bacterial cells had died. The increase in the O/C with photooxidation was due to a combination of functionalization and fragmentation reactions, which increased the O content and decreased the C content, respectively. Unsaturated compounds were observed to be more prone to reactions with ˙OH, likely through ˙OH addition to the C=C bonds. The decrease in the number of compounds detected by UPLC-MS as the photooxidation progressed highlighted the important role of fragmentation reactions. This was corroborated by the time evolution of molecular weight-fractionated compounds measured by EEM fluorescence spectroscopy, which showed that proteinaceous-like matter with molecular weights ranging from <3 kDa to >50 kDa and HULIS-like matter with molecular weights <3 kDa were released during bacterial cell damage and lysis. The time evolution of the fluorescence signals of the molecular weight-fractionated proteinaceous-like matter and HULIS-like matter indicated that lower molecular weight proteinaceous-like matter and HULIS-like matter mostly originated from fragmentation reactions of higher molecular weight proteinaceous-like matter.

Overall, our results provide new insights at the process level into the daytime interactions between live bacteria and ˙OH in clouds. These interactions can negatively impact the survival and energetic states of bacteria, which has important implications for our understanding of how bacteria influence the composition of organic matter in clouds. Microbiological–chemical interactions between organic matter and live bacteria can influence the composition of organic matter in clouds because these interactions can lead to the biodegradation of

Open Access Article. Published on 08 June 2023. Downloaded on 5/21/2026 2:53:50 AM. This article is licensed under a Creative Commons Attribution 3.0 Unported Licence.

 This journal is © The Royal Society of Chemistry 2023

Open Access Article. Published on 08 June 2023. Downloaded on 5/21/2026 2:53:50 AM. This article is licensed under a Creative Commons Attribution 3.0 Unported Licence.

small organic compounds such as organic acids, phenolic compounds, amino acids, formaldehyde, and methanol.[18,49,78–81] However, enhanced bacterial mortality due to interactions with $^{\bullet}$OH will reduce the influence of microbial activity on the composition of small organic compounds in these cloud droplets. Conversely, the release of biological and organic compounds from the bacteria during cell damage and lysis and the subsequent transformation of these compounds during photooxidation will contribute to the organic matter composition in these cloud droplets. Furthermore, the release of biological and organic compounds can occur at timescales as short as 1 h from the start of $^{\bullet}$OH-live bacterium interactions, thus highlighting the efficiency of these interactions in contributing to the organic matter composition in cloud droplets.

## Data availability

Data can be accessed by request (theodora.nah@cityu.edu.hk).

## Author contributions

Yushuo Liu: investigation, writing – original draft. Patrick K. H. Lee: conceptualization, writing – review & editing. Theodora Nah: conceptualization, writing – review & editing, supervision.

## Conflicts of interest

There is no conflict to declare.

## Acknowledgements

This work was supported by the National Natural Science Foundation of China (project number 42005081) and the Research Grants Council of the Hong Kong Special Administrative Region, China (project number 11303720).

## References

1 A. Bianco, M. Passananti, M. Brigante and G. Mailhot, Photochemistry of the Cloud Aqueous Phase: A Review, *Molecules*, 2020, **25**, 423.
2 V. F. McNeill, Aqueous organic chemistry in the atmosphere: sources and chemical processing of organic aerosols, *Environ. Sci. Technol.*, 2015, **49**, 1237–1244.
3 H. Bauer, A. Kasper-Giebl, M. Loflund, H. Giebl, R. Hitzenberger, F. Zibuschka and H. Puxbaum, The contribution of bacteria and fungal spores to the organic carbon content of cloud water, precipitation and aerosols, *Atmos. Res.*, 2002, **64**, 109–119.
4 O. Möhler, P. DeMott, G. Vali and Z. Levin, Microbiology and atmospheric processes: the role of biological particles in cloud physics, *Biogeosciences*, 2007, **4**, 1059–1071.
5 M. Vaitilingom, P. Amato, M. Sancelme, P. Laj, M. Leriche and A. M. Delort, Contribution of microbial activity to carbon chemistry in clouds, *Appl. Environ. Microbiol.*, 2010, **76**, 23–29.
6 M. Vaitilingom, L. Deguillaume, V. Vinatier, M. Sancelme, P. Amato, N. Chaumerliac and A. M. Delort, Potential impact of microbial activity on the oxidant capacity and organic carbon budget in clouds, *Proc. Natl. Acad. Sci. U. S. A.*, 2013, **110**, 559–564.
7 M. Zhang, A. Khaled, P. Amato, A. M. Delort and B. Ervens, Sensitivities to biological aerosol particle properties and ageing processes: potential implications for aerosol–cloud interactions and optical properties, *Atmos. Chem. Phys.*, 2021, **21**, 3699–3724.
8 R. Jaenicke, Abundance of cellular material and proteins in the atmosphere, *Science*, 2005, **308**, 73.
9 S. M. Burrows, W. Elbert, M. G. Lawrence and U. Poschl, Bacteria in the global atmosphere – part 1: review and synthesis of literature data for different ecosystems, *Atmos. Chem. Phys.*, 2009, **9**, 9263–9280.
10 W. Hu, H. Y. Niu, K. Murata, Z. J. Wu, M. Hu, T. Kojima and D. Z. Zhang, Bacteria in atmospheric waters: detection, characteristics and implications, *Atmos. Environ.*, 2018, **179**, 201–221.
11 P. Ariya, J. Sun, N. Eltouny, E. Hudson, C. Hayes and G. Kos, Physical and chemical characterization of bioaerosols–implications for nucleation processes, *Int. Rev. Phys. Chem.*, 2009, **28**, 1–32.
12 A.-M. Delort, M. Vaïtilingom, P. Amato, M. Sancelme, M. Parazols, G. Mailhot, P. Laj and L. Deguillaume, A short overview of the microbial population in clouds: potential roles in atmospheric chemistry and nucleation processes, *Atmos. Res.*, 2010, **98**, 249–260.
13 V. Després, J. A. Huffman, S. M. Burrows, C. Hoose, A. Safatov, G. Buryak, J. Fröhlich-Nowoisky, W. Elbert, M. Andreae, U. Pöschl and R. Jaenicke, Primary biological aerosol particles in the atmosphere: a review, *Tellus B*, 2012, **64**, 15598.
14 W. Hu, K. Murata, S. Toyonaga and D. Zhang, Bacterial abundance and viability in rainwater associated with cyclones, stationary fronts and typhoons in southwestern Japan, *Atmos. Environ.*, 2017, **167**, 104–115.
15 C. H. Xu, M. Wei, J. M. Chen, X. Sui, C. Zhu, J. R. Li, L. L. Zheng, G. D. Sui, W. J. Li, W. X. Wang, Q. Z. Zhang and A. Mellouki, Investigation of diverse bacteria in cloud water at Mt. Tai, China, *Sci. Total Environ.*, 2017, **580**, 258–265.
16 P. Amato, M. Joly, L. Besaury, A. Oudart, N. Taib, A. I. Mone, L. Deguillaume, A. M. Delort and D. Debroas, Active microorganisms thrive among extremely diverse communities in cloud water, *PLoS One*, 2017, **12**, e0182869.
17 M. Joly, P. Amato, M. Sancelme, V. Vinatier, M. Abrantes, L. Deguillaume and A.-M. Delort, Survival of microbial isolates from clouds toward simulated atmospheric stress factors, *Atmos. Environ.*, 2015, **117**, 92–98.
18 Y. Liu, C. K. Lim, Z. Shen, P. K. H. Lee and T. Nah, Effects of pH and light exposure on the survival of bacteria and their ability to biodegrade organic compounds in clouds: implications for microbial activity in acidic cloud water, *Atmos. Chem. Phys.*, 2023, **23**, 1731–1747.

Open Access Article. Published on 08 June 2023. Downloaded on 5/21/2026 2:53:50 AM. This article is licensed under a Creative Commons Attribution 3.0 Unported Licence.

19 N. Wirgot, M. Lagrée, M. Traïkia, L. Besaury, P. Amato, I. Canet, M. Sancelme, C. Jousse, B. Diémé, B. Lyan and A.-M. Delort, Metabolic modulations of Pseudomonas graminis in response to $H_2O_2$ in cloud water, *Sci. Rep.*, 2019, **9**, 12799.

20 N. Wirgot, V. Vinatier, L. Deguillaume, M. Sancelme and A. M. Delort, $H_2O_2$ modulates the energetic metabolism of the cloud microbiome, *Atmos. Chem. Phys.*, 2017, **17**, 14841–14851.

21 S. Gligorovski, R. Strekowski, S. Barbati and D. Vione, Environmental Implications of Hydroxyl Radicals (˙OH), *Chem. Rev.*, 2015, **115**, 13051–13092.

22 C. Anastasio and K. G. McGregor, Chemistry of fog waters in California's Central Valley: 1. in situ photoformation of hydroxyl radical and singlet molecular oxygen, *Atmos. Environ.*, 2001, **35**, 1079–1089.

23 A. Bianco, M. Passananti, H. Perroux, G. Voyard, C. Mouchel-Vallon, N. Chaumerliac, G. Mailhot, L. Deguillaume and M. Brigante, A better understanding of hydroxyl radical photochemical sources in cloud waters collected at the puy de Dome station – experimental versus modelled formation rates, *Atmos. Chem. Phys.*, 2015, **15**, 9191–9202.

24 R. Kaur and C. Anastasio, Light absorption and the photoformation of hydroxyl radical and singlet oxygen in fog waters, *Atmos. Environ.*, 2017, **164**, 387–397.

25 H. Herrmann, On the photolysis of simple anions and neutral molecules as sources of O−/OH, $SO_x^-$ and Cl in aqueous solution, *Phys. Chem. Chem. Phys.*, 2007, **9**, 3935–3964.

26 D. Vione, V. Maurino, C. Minero, E. Pelizzetti, M. A. J. Harrison, R. I. Olariu and C. Arsene, Photochemical reactions in the tropospheric aqueous phase and on particulate matter, *Chem. Soc. Rev.*, 2006, **35**, 441–453.

27 A. D. Estillore, J. V. Trueblood and V. H. Grassian, Atmospheric chemistry of bioaerosols: heterogeneous and multiphase reactions with atmospheric oxidants and other trace gases, *Chem. Sci.*, 2016, **7**, 6604–6616.

28 T. Nah, S. H. Kessler, K. E. Daumit, J. H. Kroll, S. R. Leone and K. R. Wilson, OH-initiated oxidation of sub-micron unsaturated fatty acid particles, *Phys. Chem. Chem. Phys.*, 2013, **15**, 18649–18663.

29 T. Nah, S. H. Kessler, K. E. Daumit, J. H. Kroll, S. R. Leone and K. R. Wilson, Influence of Molecular Structure and Chemical Functionality on the Heterogeneous OH-Initiated Oxidation of Unsaturated Organic Particles, *J. Phys. Chem. A*, 2014, **118**, 4106–4119.

30 T. Nah, H. F. Zhang, D. R. Worton, C. R. Ruehl, B. B. Kirk, A. H. Goldstein, S. R. Leone and K. R. Wilson, Isomeric Product Detection in the Heterogeneous Reaction of Hydroxyl Radicals with Aerosol Composed of Branched and Linear Unsaturated Organic Molecules, *J. Phys. Chem. A*, 2014, **118**, 11555–11571.

31 E. Stadtman, Oxidation of free amino acids and amino acid residues in proteins by radiolysis and by metal-catalyzed reactions, *Annu. Rev. Biochem.*, 1993, **62**, 797–821.

32 F. Liu, S. Lai, H. Tong, P. S. J. Lakey, M. Shiraiwa, M. G. Weller, U. Pöschl and C. J. Kampf, Release of free amino acids upon oxidation of peptides and proteins by hydroxyl radicals, *Anal. Bioanal. Chem.*, 2017, **409**, 2411–2420.

33 B. S. Berlett and E. R. Stadtman, Protein oxidation in aging, disease, and oxidative stress, *J. Biol. Chem.*, 1997, **272**, 20313–20316.

34 T. Li, Z. Wang, Y. Wang, C. Wu, Y. Liang, M. Xia, C. Yu, H. Yun, W. Wang, Y. Wang, J. Guo, H. Herrmann and T. Wang, Chemical characteristics of cloud water and the impacts on aerosol properties at a subtropical mountain site in Hong Kong SAR, *Atmos. Chem. Phys.*, 2020, **20**, 391–407.

35 V. Shah, D. J. Jacob, J. M. Moch, X. Wang and S. Zhai, Global modeling of cloud water acidity, precipitation acidity, and acid inputs to ecosystems, *Atmos. Chem. Phys.*, 2020, **20**, 12223–12245.

36 X. Wu, S. Monchy, S. Taghavi, W. Zhu, J. Ramos and D. van der Lelie, Comparative genomics and functional analysis of niche-specific adaptation in Pseudomonas putida, *FEMS Microbiol. Rev.*, 2011, **35**, 299–323.

37 A. M. Earl, R. Losick and R. Kolter, Ecology and genomics of Bacillus subtilis, *Trends Microbiol.*, 2008, **16**, 269–275.

38 L. Deguillaume, T. Charbouillot, M. Joly, M. Vaïtilingom, M. Parazols, A. Marinoni, P. Amato, A. M. Delort, V. Vinatier, A. Flossmann, N. Chaumerliac, J. M. Pichon, S. Houdier, P. Laj, K. Sellegri, A. Colomb, M. Brigante and G. Mailhot, Classification of clouds sampled at the puy de Dôme (France) based on 10 years of monitoring of their physicochemical properties, *Atmos. Chem. Phys.*, 2014, **14**, 1485–1506.

39 A. Marinoni, M. Parazols, M. Brigante, L. Deguillaume, P. Amato, A.-M. Delort, P. Laj and G. Mailhot, Hydrogen peroxide in natural cloud water: Sources and photoreactivity, *Atmos. Res.*, 2011, **101**, 256–263.

40 D. van Pinxteren, K. W. Fomba, S. Mertes, K. Müller, G. Spindler, J. Schneider, T. Lee, J. L. Collett and H. Herrmann, Cloud water composition during HCCT-2010: Scavenging efficiencies, solute concentrations, and droplet size dependence of inorganic ions and dissolved organic carbon, *Atmos. Chem. Phys.*, 2016, **16**, 3185–3205.

41 M. Koutny, M. Sancelme, C. Dabin, N. Pichon, A.-M. Delort and J. Lemaire, Acquired biodegradability of polyethylenes containing pro-oxidant additives, *Polym. Degrad. Stab.*, 2006, **91**, 1495–1503.

42 Y. Lyu, J. T. C. Chow and T. Nah, Kinetics of the nitrate-mediated photooxidation of monocarboxylic acids in the aqueous phase, *Environ. Sci.: Processes Impacts*, 2023, **25**, 461–471.

43 J. Yang, W. C. Au, H. Law, C. H. Leung, C. H. Lam and T. Nah, pH affects the aqueous-phase nitrate-mediated photooxidation of phenolic compounds: implications for brown carbon formation and evolution, *Environ. Sci.: Processes Impacts*, 2023, **25**, 176–189.

44 J. W. Yang, W. C. Au, H. Law, C. H. Lam and T. Nah, Formation and evolution of brown carbon during aqueous-

Open Access Article. Published on 08 June 2023. Downloaded on 5/21/2026 2:53:50 AM.
This article is licensed under a Creative Commons Attribution 3.0 Unported Licence.

phase nitrate-mediated photooxidation of guaiacol and 5-nitroguaiacol, *Atmos. Environ.*, 2021, **254**, 118401.

45 A. Lallement, V. Vinatier, M. Brigante, L. Deguillaume, A. M. Delort and G. Mailhot, First evaluation of the effect of microorganisms on steady state hydroxyl radical concentrations in atmospheric waters, *Chemosphere*, 2018, **212**, 715–722.

46 H. Herrmann, D. Hoffmann, T. Schaefer, P. Bräuer and A. Tilgner, Tropospheric Aqueous-Phase Free-Radical Chemistry: Radical Sources, Spectra, Reaction Kinetics and Prediction Tools, *ChemPhysChem*, 2010, **11**, 3796–3822.

47 R. Helmus, T. L. Ter Laak, A. P. van Wezel, P. de Voogt and E. L. Schymanski, patRoon: open source software platform for environmental mass spectrometry based non-target screening, *J. Cheminf.*, 2021, **13**, 1–25.

48 J. P. S. Wong, M. Tsagkaraki, I. Tsiodra, N. Mihalopoulos, K. Violaki, M. Kanakidou, J. Sciare, A. Nenes and R. J. Weber, Atmospheric evolution of molecular-weight-separated brown carbon from biomass burning, *Atmos. Chem. Phys.*, 2019, **19**, 7319–7334.

49 M. Vaïtilingom, T. Charbouillot, L. Deguillaume, R. Maisonobe, M. Parazols, P. Amato, M. Sancelme and A. M. Delort, Atmospheric chemistry of carboxylic acids: microbial implication versus photochemistry, *Atmos. Chem. Phys.*, 2011, **11**, 8721–8733.

50 A. Bianco, L. Deguillaume, N. Chaumerliac, M. Vaitilingom, M. Wang, A. M. Delort and M. C. Bridoux, Effect of endogenous microbiota on the molecular composition of cloud water: a study by Fourier-transform ion cyclotron resonance mass spectrometry (FT-ICR MS), *Sci. Rep.*, 2019, **9**, 7663.

51 A. P. Blanchard, M. R. Bird and S. J. L. Wright, Peroxygen disinfection of Pseudomonas aeruginosa biofilms on stainless steel discs, *Biofouling*, 1998, **13**, 233–253.

52 S. B. Farr and T. Kogoma, Oxidative stress responses in Escherichia coli and Salmonella typhimurium, *Microbiol. Rev.*, 1991, **55**, 561–585.

53 E. S. Henle and S. Linn, Formation, prevention, and repair of DNA damage by iron/hydrogen peroxide, *J. Biol. Chem.*, 1997, **272**, 19095–19098.

54 F. C. Fang, Perspectives series: host/pathogen interactions. Mechanisms of nitric oxide-related antimicrobial activity, *J. Clin. Invest.*, 1997, **99**, 2818–2825.

55 R. Moeller, P. Setlow, G. n. Reitz and W. L. Nicholson, Roles of small, acid-soluble spore proteins and core water content in survival of Bacillus subtilis spores exposed to environmental solar UV radiation, *Appl. Environ. Microbiol.*, 2009, **75**, 5202–5208.

56 D. Wang, T. Oppenländer, M. G. El-Din and J. R. Bolton, Comparison of the disinfection effects of vacuum-UV (VUV) and UV light on Bacillus subtilis spores in aqueous suspensions at 172, 222 and 254 nm, *Photochem. Photobiol.*, 2010, **86**, 176–181.

57 G. Wu, P. Fu, K. Ram, J. Song, Q. Chen, K. Kawamura, X. Wan, S. Kang, X. Wang, A. Laskin and Z. Cong, Fluorescence characteristics of water-soluble organic carbon in atmospheric aerosol☆, *Environ. Pollut.*, 2021, **268**, 115906.

58 C. Pöhlker, J. Huffman and U. Pöschl, Autofluorescence of atmospheric bioaerosols–fluorescent biomolecules and potential interferences, *Atmos. Meas. Tech.*, 2012, **5**, 37–71.

59 Q. Chen, Y. Miyazaki, K. Kawamura, K. Matsumoto, S. Coburn, R. Volkamer, Y. Iwamoto, S. Kagami, Y. Deng and S. Ogawa, Characterization of chromophoric water-soluble organic matter in urban, forest, and marine aerosols by HR-ToF-AMS analysis and excitation–emission matrix spectroscopy, *Environ. Sci. Technol.*, 2016, **50**, 10351–10360.

60 S. Yue, L. Ren, T. Song, L. Li, Q. Xie, W. Li, M. Kang, W. Zhao, L. Wei and H. Ren, Abundance and diurnal trends of fluorescent bioaerosols in the troposphere over Mt. Tai, China, in spring, *J. Geophys. Res.: Atmos.*, 2019, **124**, 4158–4173.

61 A. Bianco, M. Passananti, L. Deguillaume, G. Mailhot and M. Brigante, Tryptophan and tryptophan-like substances in cloud water: occurrence and photochemical fate, *Atmos. Environ.*, 2016, **137**, 53–61.

62 M. Kuwata, W. Shao, R. Lebouteiller and S. T. Martin, Classifying organic materials by oxygen-to-carbon elemental ratio to predict the activation regime of Cloud Condensation Nuclei (CCN), *Atmos. Chem. Phys.*, 2013, **13**, 5309–5324.

63 A. P. Bateman, S. A. Nizkorodov, J. Laskin and A. Laskin, Photolytic processing of secondary organic aerosols dissolved in cloud droplets, *Phys. Chem. Chem. Phys.*, 2011, **13**, 12199–12212.

64 G. D. Chen, S. Hanukovich, M. Chebeir, P. Christopher and H. Z. Liu, Nitrate Removal via a Formate Radical-Induced Photochemical Process, *Environ. Sci. Technol.*, 2019, **53**, 316–324.

65 R. F. Zhang, M. S. Gen, T. M. Fu and C. K. Chan, Production of Formate via Oxidation of Glyoxal Promoted by Particulate Nitrate Photolysis, *Environ. Sci. Technol.*, 2021, **55**, 5711–5720.

66 E. Ford, M. N. Hughes and P. Wardman, Kinetics of the reactions of nitrogen dioxide with glutathione, cysteine, and uric acid at physiological pH, *Free Radical Biol. Med.*, 2002, **32**, 1314–1323.

67 J. M. Fukuto, S. J. Carrington, D. J. Tantillo, J. G. Harrison, L. J. Ignarro, B. A. Freeman, A. Chen and D. A. Wink, Small molecule signaling agents: the integrated chemistry and biochemistry of nitrogen oxides, oxides of carbon, dioxygen, hydrogen sulfide, and their derived species, *Chem. Res. Toxicol.*, 2012, **25**, 769–793.

68 L. F. Gamon and U. Wille, Oxidative damage of biomolecules by the environmental pollutants $NO_2^{\bullet}$ and $NO_3^{\bullet}$, *Acc. Chem. Res.*, 2016, **49**, 2136–2145.

69 C. L. Heald, J. H. Kroll, J. L. Jimenez, K. S. Docherty, P. F. DeCarlo, A. C. Aiken, Q. Chen, S. T. Martin, D. K. Farmer and P. Artaxo, A simplified description of the evolution of organic aerosol composition in the atmosphere, *Geophys. Res. Lett.*, 2010, **37**, L08803.

Open Access Article. Published on 08 June 2023. Downloaded on 5/21/2026 2:53:50 AM.
This article is licensed under a Creative Commons Attribution 3.0 Unported Licence.

70 J. H. Kroll, N. M. Donahue, J. L. Jimenez, S. H. Kessler, M. R. Canagaratna, K. R. Wilson, K. E. Altieri, L. R. Mazzoleni, A. S. Wozniak, H. Bluhm, E. R. Mysak, J. D. Smith, C. E. Kolb and D. R. Worsnop, Carbon oxidation state as a metric for describing the chemistry of atmospheric organic aerosol, *Nat. Chem.*, 2011, **3**, 133–139.

71 C. P. West, A. C. Morales, J. Ryan, M. V. Misovich, A. P. S. Hettiyadura, F. Rivera-Adorno, J. M. Tomlin, A. Darmody, B. N. Linn, P. Lin and A. Laskin, Molecular investigation of the multi-phase photochemistry of Fe(iii)–citrate in aqueous solution, *Environ. Sci.: Processes Impacts*, 2023, **25**, 190–213.

72 P. Renard, A. Bianco, J. Jänis, T. Kekäläinen, M. Bridoux and L. Deguillaume, Puy de Dôme Station (France): A Stoichiometric Approach to Compound Classification in Clouds, *J. Geophys. Res.: Atmos.*, 2022, **127**, e2022JD036635.

73 B. Buszewski and S. Noga, Hydrophilic interaction liquid chromatography (HILIC)–a powerful separation technique, *Anal. Bioanal. Chem.*, 2012, **402**, 231–247.

74 A. Bator and J. L. Collett Jr, Cloud chemistry varies with drop size, *J. Geophys. Res.: Atmos.*, 1997, **102**, 28071–28078.

75 K. F. Moore, D. E. Sherman, J. E. Reilly and J. L. Collett, Drop size-dependent chemical composition in clouds and fogs. Part I. Observations, *Atmos. Environ.*, 2004, **38**, 1389–1402.

76 X. Shen, T. Lee, J. Guo, X. Wang, P. Li, P. Xu, Y. Wang, Y. Ren, W. Wang, T. Wang, Y. Li, S. A. Carn and J. L. Collett, Aqueous phase sulfate production in clouds in eastern China, *Atmos. Environ.*, 2012, **62**, 502–511.

77 T. Arakaki, T. Miyake, T. Hirakawa and H. Sakugawa, pH dependent photoformation of hydroxyl radical and absorbance of aqueous-phase N(III) ($HNO_2$ and $NO_2^-$), *Environ. Sci. Technol.*, 1999, **33**, 2561–2565.

78 P. A. Ariya, O. Nepotchatykh, O. Ignatova and M. Amyot, Microbiological degradation of atmospheric organic compounds, *Geophys. Res. Lett.*, 2002, **29**, 2077.

79 S. Husárová, M. Vaïtilingom, L. Deguillaume, M. Traikia, V. Vinatier, M. Sancelme, P. Amato, M. Matulová and A.-M. Delort, Biotransformation of methanol and formaldehyde by bacteria isolated from clouds. Comparison with radical chemistry, *Atmos. Environ.*, 2011, **45**, 6093–6102.

80 S. Jaber, M. Joly, M. Brissy, M. Leremboure, A. Khaled, B. Ervens and A.-M. Delort, Biotic and abiotic transformation of amino acids in cloud water: experimental studies and atmospheric implications, *Biogeosciences*, 2021, **18**, 1067–1080.

81 S. Jaber, A. Lallement, M. Sancelme, M. Leremboure, G. Mailhot, B. Ervens and A.-M. Delort, Biodegradation of phenol and catechol in cloud water: comparison to chemical oxidation in the atmospheric multiphase system, *Atmos. Chem. Phys.*, 2020, **20**, 4987–4997.

 This journal is © The Royal Society of Chemistry 2023